University of Nebraska - Lincoln
DigitalCommons@University of Nebraska - Lincoln

US Department of Energy Publications | U.S. Department of Energy

2001

Solubilization of Fe(III) oxide-bound trace metals by a dissimilatory Fe(III) reducing bacterium

John M. Zachara
Pacific Northwest National Laboratory, john.zachara@pnl.gov

James K. Fredrickson
Pacific Northwest National Laboratory, jim.fredrickson@pnl.gov

Steven Smith
Pacific Northwest National Laboratory, steven.smith@pnl.gov

Paul Gassman
Pacific Northwest National Laboratory, paul.gassman@pnl.gov

Follow this and additional works at: http://digitalcommons.unl.edu/usdoepub

 Part of the Bioresource and Agricultural Engineering Commons

Zachara, John M.; Fredrickson, James K.; Smith, Steven; and Gassman, Paul, "Solubilization of Fe(III) oxide-bound trace metals by a dissimilatory Fe(III) reducing bacterium" (2001). *US Department of Energy Publications*. 249.
http://digitalcommons.unl.edu/usdoepub/249

This Article is brought to you for free and open access by the U.S. Department of Energy at DigitalCommons@University of Nebraska - Lincoln. It has been accepted for inclusion in US Department of Energy Publications by an authorized administrator of DigitalCommons@University of Nebraska - Lincoln.

This article is a U.S. government work, and is not subject to copyright in the United States.

Pergamon

Geochimica et Cosmochimica Acta, Vol. 65, No. 1, pp. 75–93, 2001
Copyright © 2001 Elsevier Science Ltd
Printed in the USA. All rights reserved
0016-7037/01 $20.00 + .00

PII S0016-7037(00)00500-7

Solubilization of Fe(III) oxide-bound trace metals by a dissimilatory Fe(III) reducing bacterium

JOHN M. ZACHARA,* JIM K. FREDRICKSON, STEVEN C. SMITH, and PAUL L. GASSMAN
Pacific Northwest National Laboratory, MSIN K8-96, P.O. Box 999, Richland, WA 99352, USA

(*Received December* 11, 1999; *accepted in revised form May* 30, 2000)

Abstract—Trace metals associate with Fe(III) oxides as adsorbed or coprecipitated species, and consequently, the biogeochemical cycles of iron and the trace metals are closely linked. This communication investigated the solubilization of coprecipitated Co(III) and Ni(II) from goethite (α-FeOOH) during dissimilatory bacterial iron reduction to provide insights on biogeochemical factors controlling trace-element fluxes in anoxic environments. Suspensions of homogeneously substituted Co-FeOOH (50 mmol/L as $Co_{0.01}Fe_{0.99}OOH$; ^{57}Co-labeled) in eight different buffer/media solutions were inoculated with a facultative, metal-reducing bacteria isolated from groundwater (*Shewanella putrefacians* CN32), and incubated under strictly anaerobic conditions for periods up to 32 days. Lactate (30 mmol/L) was provided as an electron donor. Growth and non-growth promoting conditions were established by adding or withholding PO_4 and/or trace metals (^{60}Co-labeled) from the incubation media. Anthraquinone disulfonate (AQDS; 100 μmol/L) was added to most suspensions as an electron shuttle to enhance bacterial reduction. Solutions were buffered at circumneutral pH with either PIPES or bicarbonate buffers. Solid and liquid samples were analyzed at intermediate and final time points for aqueous and sorbed/precipitated (by HCl extraction) Fe(II) and Co(II). The bioreduced solids were analyzed by X-ray diffraction and field-emission electron microscopy at experiment termination. Ni-FeOOH ($Ni_{0.01}Fe_{0.99}OOH$) was used for comparison in select experiments. Up to 45% of the metal containing FeOOH was bioreduced; growth-supporting conditions did not enhance reduction. The biogenic Fe(II) strongly associated with the residual Fe(III) oxide as an undefined sorbed phase at low fractional reduction in PIPES buffer, and as siderite ($FeCO_3$) in bicarbonate buffer or as vivianite [$Fe_3(PO_4)_2 \cdot 8H_2O$] when P was present. Cobalt(III) was reduced to Co(II) in proportion to its mole ratio in the solid. The release of bioreduced Co(II) to the aqueous phase showed complex dependency on the media and buffer composition and the fractional reduction of the Co-FeOOH. In most cases Co(II) was solubilized in preference to Fe(II), but in select cases it was not. These differences were rationalized in terms of competitive adsorption reactions on the residual Fe(III) oxide surface and coprecipitation in biogenic Fe(II) solids. The bioreduced Co-FeOOH surface showed unexpectedly high sorption selectivity for the biomobilized Co(II). The bioreductive solubilization of Ni(II) from Ni-FeOOH was comparable to Co-FeOOH. Our results indicate that Fe(III)-oxide-entrained trace metals can be mobilized during bacterial iron reduction leading to a net increase, in most cases, in aqueous metal concentrations. The enhancement in trace-metal aqueous concentration, e.g., in groundwater, may proportionally exceed that of Fe(II). *Copyright © 2001 Elsevier Science Ltd*

1. INTRODUCTION

Iron (III) oxides are common mineral components of soils, sediments, aquifers, and geologic materials. Fe(III) oxides form as secondary weathering products, and may exist as intergrain cements, particle coatings of complex and varied composition, and as discrete amorphous or crystalline phases (Schwertmann and Taylor, 1989). Natural Fe(III) oxides are high in surface area and are reactive (Cornell and Schwertmann, 1996). The sorption and redox chemistry of Fe(III) oxides has been well studied (see Cornell and Schwertmann, 1996) because of recognition that they control water chemistry and contaminant behavior in near-surface geochemical systems. Fe(III) oxides sorb a wide range of metal cations and anions by complexation to surface hydroxyl groups (Schindler and Stumm, 1987), and function as the primary redox buffering solid phase in many sediments and subsurface materials (Heron et al., 1994).

The iron biogeochemical cycle is intimately linked with those of C, S, O, and N, and is a primary pathway for energy and electron flux in near surface environments (Stumm and Sulzberger, 1992). Because Fe(III) is insoluble (e.g., Lindsay, 1979), Fe(III) oxides are the primary repository of oxidized iron in near surface environments. The reductive portion of the iron biogeochemical cycle in nonphototropic environments (e.g., sediments and subsurface materials) is driven by the direct enzymatic reduction of Fe(III) oxides to Fe(II) by dissimilatory iron reducing bacteria (DIRB; Lovley et al., 1991; Lovley, 1993), or indirectly via the redox cycling of humic acids (Lovley et al., 1996; Lovley et al., 1998). The iron biogeochemical cycle links with those of the trace metals through speciation effects, as many trace metals co-associate with Fe(III) oxides or reduced iron phases (e.g., magnetite, siderite, or iron sulfide) when they exist. This paper is concerned with the linkage of the Fe and trace-metal biogeochemical cycles, specifically with regard to the biogeochemistry of Co and Ni coprecipitated with Fe(III) oxide.

Valence II and III metal cations can isomorphously substitute in the crystalline Fe(III) oxide structure (e.g., goethite and hematite; Cornell and Schwertmann, 1996). The potential for substitution is determined by the similarity in ionic radius and valency of the foreign ion, and their electronic properties as

* Author to whom correspondence should be addressed (john.zachara@pnl.gov).

compared to that of high-spin Fe(III). Substitution changes the unit-cell edge length and volume of the Fe(III) oxide (Gerth, 1990), and may effect the average crystallite size and aspect ratio, particle morphology, surface area, solubility (Trolard and Tardy, 1987), surface chemistry (Ainsworth et al., 1989), and rates of acid and reductive dissolution (Torrent et al., 1987; Schwertmann, 1991). Aluminum (III) is the most readily substituted metal cation in both hematite and goethite (Cornell and Schwertmann, 1996), and Al-substituted crystalline oxides are common in soil and sediment. The trace metals Cr(III), V(III), Mn(III), Ni(II), Cu(II), Zn(II), and Cd(II) all substitute in laboratory synthesized goethite to levels below 10% (Cornell and Schwertmann, 1996). Chemical analyses of soil materials indicates that isomorphous substitution of minor elements in crystalline Fe(III) oxides occurs in nature (Singh and Gilkes, 1992; Trolard et al., 1995).

DIRB can utilize both noncrystalline and crystalline Fe(III) oxides as terminal electron acceptors for respiration (Roden and Zachara, 1996; Fredrickson et al., 1998; Zachara et al., 1998); thereby reducing all or a fraction of the solid. The primary inorganic product of bacterial iron reduction is ferrous iron (Fe^{2+}), although CO_2 is also generated by oxidation of organic carbon. Biogenic Fe^{2+} may undergo a series of post-reduction biogeochemical reactions including sorption to bacteria, the residual Fe(III) oxide surface, and/or co-associated mineral phases; surface precipitation on the oxide surface; and/or the formation of discrete ferrous solid phases such as siderite, magnetite, green rust, and vivianite (Zachara et al., 1998; Fredrickson et al., 1998; Urrutia et al., 1998; Zachara et al., 1999). The extent and identity of these reactions is dependent on the nature of co-associated solids and the chemical composition of the aqueous phase including type and concentration of buffer (e.g., HCO_3), nutrient ions (e.g., PO_4), and the presence or absence of complexants. These postreduction geochemical reactions of Fe^{2+} may influence the disposition of minor elements associated with the Fe(III) oxide. Bousserrhine et al. (1999) investigated the solubilization of co-precipitated metals (Co and Mn) from goethite during glucose fermentation and found that metal release was congruent with that of Fe(II) under the acidic conditions that developed.

In this communication, we investigate the fate of oxide-entrained trace metals (Co, Ni) during the bioreduction of synthetic, metal-substituted crystalline Fe(III) oxides (goethite; $Co_{0.01}Fe_{0.99}OOH$, $Ni_{0.01}Fe_{0.99}OOH$) at circumneutral pH. A DIRB (*Shewanella putrefacians*, CN32) is utilized that is known to reduce crystalline Fe(III) oxides and nucleate a variety of post-reduction ferrous iron solids depending on buffer and media composition (Zachara et al., 1998; Fredrickson et al., 1998). Different buffer and media treatments were used to investigate the biogeochemical phenomena that could be operative. We explore whether the release rate of the entrained trace metals is equal to their mole fraction substitution, and evaluate geochemical causes (e.g., sorption, precipitation) for disparities. An overall assessment is provided as to whether oxide entrained trace metals are likely to be mobilized or immobilized during bacterial Fe(III) oxide reduction, thereby providing insights on the biogeochemical cycling of trace metals under anoxic conditions with implications to the bioremediation of metal-contaminated lands and subsurface environments.

2. MATERIALS AND EXPERIMENTAL METHODS

2.1. General Conditions

Laboratory prepared goethite containing either 1 mol percent Co or Ni was incubated anaerobically with *S. putrefaciens* strain CN32. The suspensions contained 50 mmol/L synthetic oxide and eight media treatments (Table 1). Four replicates of inoculated and non-inoculated treatments were sampled at selected time intervals ranging out to 32 days. Suspension pH; aqueous HCO_3^-; and aqueous and HCl-extractable Fe(II), Fe(III), PO_4 (aqueous-only), and Ni and Co were determined; and subsamples of the reduced solid were analyzed microscopically and by X-ray diffraction.

2.2. Preparation of Co-FeOOH and Ni-FeOOH

Goethite containing either 1 mol.% Co or Ni was prepared by combining 2.7 L of 1 mol/L KOH (Sigma, St. Louis, MO, USA) with either 0.3 L of 0.99 mol/L $Fe(NO_3)_3$ (Sigma) and 0.01 mol/L $Co(NO_3)_2$ or 0.3 L of 0.99 mol/L $Fe(NO_3)_3$ (Sigma), and 0.01 mol/L $Ni(NO_3)$ in a 4-L Nalgene (HDPE) bottle previously rinsed with 1 mol/L KOH. The solution was placed in a 75°C oven for 7 days with daily mixing. After the 7-day incubation period, the solid was washed five times with hydroxylamine hydrochloride solution (0.25 mol/L $NH_2OH \cdot HCl$ in 0.25 mol/L HCl at 50°C) to remove ferrihydrite and five times with 0.1 mol/L $NaClO_4$. The solids were resuspended in 0.1 mol/L $NaClO_4$ and dialyzed against deionized water by using Spectrapor 7 (1000 MWCO) cellulose tubing. The dialyzed suspensions were lyophilized and stored under N_2. A portion of the solids was dissolved in Ultrex HCl and the concentrations of Fe, Co, and Ni determined using inductively coupled plasma argon emission spectroscopy (ICP-AES). The results confirmed an approximate 1 : 100 ratio of either Co : Fe or Ni : Fe. The surface areas of the lyophilized Co-FeOOH and Ni-FeOOH were determined by multipoint BET analysis with N_2 as the adsorbate (Quantachrome Corporation, Syosset, N.Y.) yielding 11.73 m^2/g and 55.73 m^2/g for the Ni-FeOOH and Co-FeOOH, respectively.

Goethite containing 1 mol.% Co radiolabeled with ^{57}Co was prepared by combining 1.34 L of 1 M KOH (Sigma) with 0.13 L of 0.99 M $Fe(NO_3)_3$ (Sigma) and 0.01 M $Co(NO_3)_2$ (Sigma) with 1 millicurie ^{57}Co as $CoCl_2$ (DuPont, Wilmington, DE, USA) in a 4-L Nalgene (HDPE) bottle previously rinsed with 1 M KOH. The suspension was then treated identically as described for the synthesis of Co- and Ni-FeOOH. Residual ferrihydrite was extracted with hydroxylamine hydrochloride and the washed solid was stored at 4°C in a Nalgene (HDPE) bottle.

2.3. Dissolution of Ni-FeOOH and Co-FeOOH

Lyophilized Ni-FeOOH or Co-FeOOH (250 mg/L) was added to 6 mol/L Ultrex HCl and mixed continuously at room temperature. Aliquots of suspension were removed at 1, 2, 3, 4, 5, 6, 7, 10, 24, 48, and 120 h and passed through a 0.2-μm filter. Filtrates were analyzed by inductively coupled plasma mass spectroscopy (ICP-MS) to determine the dissolved concentrations of Fe and Ni or Co. Dissolution of the solids was complete within 24 h.

2.4. Preparation of Goethite Suspensions and Growth Media Solutions

Two 100 mmol/L stock suspensions of either Co-FeOOH or Ni-FeOOH were anoxically prepared in 0.1 mol/L $NaClO_4$. The suspensions were sonicated for 1 h on 2 consecutive days prior to use. A summary of the media components is presented in Table 1. The pH of each solution was adjusted to 7.0 and filter sterilized using a 0.2-μm filter.

Five mL of goethite suspension were added to tared headspace vials, the vials weighed, and 4 mL of the desired microbial growth media added. To reduce the O_2 present in the system, a stream of O_2-free N_2:CO_2 or N_2, determined by the media treatment (Table 1), was passed over the suspension in each vial for ~5 min after which the vial was tightly sealed to minimize intrusion of O_2.

Table 1. Media treatments for bioreduction of Co-FeOOH.

Headspace atmosphere	Media #1 Nitrogen: Carbon dioxide (80:20)	Media #2 Nitrogen: Carbon dioxide (80:20)	Media #3 Nitrogen	Media #4 Nitrogen	Media #5 Nitrogen: Carbon dioxide (80:20)	Media #6 Nitrogen: Carbon dioxide (80:20)
Basic media (mmol/L)						
ammonium chloride	28.0	28.0	28.0	28.0	28.0	28.0
potassium chloride	1.34	1.34	1.34	1.34	1.34	1.34
calcium chloride	0.68	0.68	0.68	0.68	0.68	0.68
sodium perchlorate	50.0	50.0	50.0	50.0	50.0	50.0
AQDS[a]	0.10	0.10	0.10	0.10	0.10	0.10
lactate	30.0	30.0	30.0	30.0	30.0	30.0
phosphate	4.35	0	4.35	0	4.35	0
pH Buffer (mmol/L)						
sodium bicarbonate	29.8	29.8	0	0	29.8	29.8
PIPES[b]	0	0	10.0	10.0	0	0
Trace metals (μmol/L)						
nitriloacetic acid[c]	78.5	78.5	78.5	78.5	0	0
magnesium sulfate	131	131	131	131	0	0
sodium chloride	171	171	171	171	0	0
manganese sulfate	29.7	29.7	29.7	29.7	0	0
zinc chloride	9.53	9.53	9.53	9.53	0	0
ferrous sulfate	3.07	3.07	3.07	3.07	0	0
calcium chloride	9.01	9.01	9.01	9.01	0	0
sodium molybdate	1.24	1.24	1.24	1.24	0	0
sodium tungstate	1.02	1.02	1.02	1.02	0	0
nickel chloride	0.84	0.84	0.84	0.84	0	0
cupric sulfate	0.40	0.40	0.40	0.40	0	0
aluminum potassium disulfate	0.21	0.21	0.21	0.21	0	0
boric acid	1.62	1.62	1.62	1.62	0	0
cobaltous perchlorate[d]	1.00	1.00	1.00	1.00	0	0
Media pH (with HCl or NaOH)	7.0	7.0	7.0	7.0	7.0	7.0

[a] AQDS = Anthraquinone-2,6-disulfonic acid disodium salt (fw = 412.31 g).
[b] PIPES = Piperazine-N,N′-bis(ethanesulfonic acid) (fw = 302.4 g).
[c] Nitriloacetic acid = N,N-bis(carboxymethyl)glycine (fw = 191.14 g).
[d] Radiolabeled with ^{60}Co.

2.5. Preparation of Bacterial Cultures

The *S. putrefaciens* strain CN32 was originally isolated from anoxic aquifer sediments (Fredrickson et al., 1997) and cultures were provided by Dr. David Boone at Portland State University. The cells were aerobically cultured in tryptic soy broth media without dextrose and harvested at late log growth phase by centrifuging the suspension at 5860 rcf (relative centrifugal force) for 10 min at 4°C. The cells were washed three times with sterile, O_2-free $NaHCO_3$ solution (2.5 g/L). Following the last wash the cells were resuspended in either anoxic $NaHCO_3$ or PIPES solution for inoculation of bicarbonate or PIPES-buffered media treatments, respectively. The microbial cell density was adjusted to $\sim 10^9$ cfu/mL. The final cell density was determined by staining cells with acridine orange and counting with fluorescence microscopy.

2.6. Inoculation and Incubation

Either 1 mL of CN32 culture or 1 mL of degassed, deionized water was aseptically and anoxically added to each vial as appropriate. The vials were placed (horizontally) in an incubator shaker set for 100 rpm and 30°C, and kept in darkness until sampled.

2.7. Sampling and Analyses

The vials were weighed to obtain a total suspension mass before further processing. To ensure homogeneity before sampling, each suspension was vortex-mixed for ~30 s and returned to an anoxic chamber. Samples of the aqueous phase were obtained by combining 3 mL of suspension of two replicates in a 10-mL plastic syringe fitted with a 0.2-μm filter. The first 20 drops of filtrate were discarded. Three mL of aqueous filtrate was combined with 1 mL of 3 mol/L HCl. Acid extractable components were determined by combining 1 mL of suspension from each of two replicates with 0.67 mL of 3 mol/L HCl and 7.3 mL of water. The suspension was in contact with 0.2 mol/L HCl overnight, then filtered as described above. The remaining suspension from three replicates was combined in an Oakridge polycarbonate centrifuge tube and centrifuged to concentrate the solids. The solids were washed 1× with anoxic 0.1 mol/L $NaClO_4$. The washed solid was transferred to a glass slide and covered with glycerol before analysis by X-ray diffraction. The fourth replicate was set aside for microscopic analysis.

The suspension pH was determined by using an Orion (Boston, MA, USA) pH meter/Microelectrode, Inc. (Londonderry, NH, USA) combination pH electrode calibrated using pH and 4.01 buffers. Carbon was determined by ultraviolet-promoted persulfate oxidation using a carbon analyzer (DC-80; Dohrmann Analytical Equipment Co., Santa Clara, CA, USA). Total carbon, dissolved organic carbon, and dissolved inorganic carbon were determined by varying the instrument's operating condition during multiple sample injections. Near the detection limit (typically 1.67×10^{-5} mol/L-C) the normal error is ±25%. Analytical results above 8.33×10^{-5} mol/L-C typically have <5% error. Phosphate concentration in the 0.2-μm filtrates was determined by using a colorimetric procedure involving ammonium molybdate, antimony potassium tartrate, and ascorbic acid (Olsen and Sommers, 1982) and was made within 48 h to ensure sample integrity. The intensity of color development was determined at 850 nm after 30 min and within 24 h after combining the sample with the reagents. The lowest concentration of P used in the development of a standard curve was 1.6×10^{-6} mol/L. A five point standard curve ($r^2 = 0.99$) spanning the range of 1.6×10^{-6} to 3.3×10^{-5} mol/L-P produced errors of 2% or less from the known P concentrations.

The Fe(II) concentrations in the aqueous phase, and HCl extracts

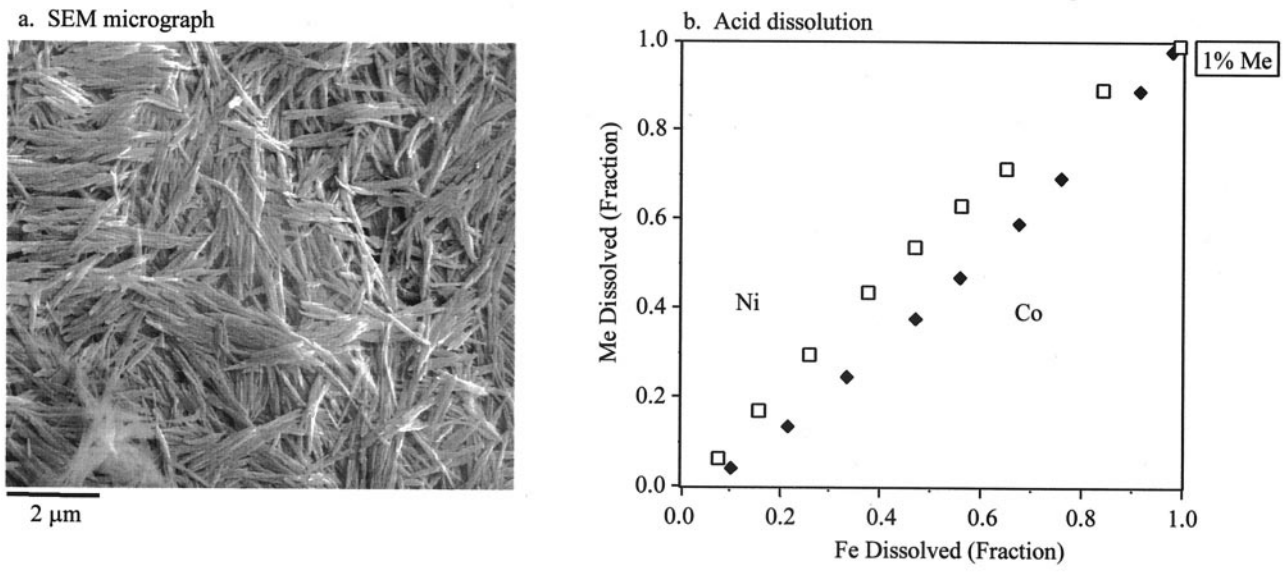

Fig. 1. Electron micrograph of Co-FeOOH (a) and acid dissolution in 6 N HCl (b) of Co- and Ni-FeOOH showing approximate congruent release of Co, Ni, and Fe.

were determined using a colorimetric procedure employing ferrozine {[3-(2-pyridyl)-5,6-bis(4-phenylsulfonic acid)-1,2,4-triazine monosodium salt], 1 g/L} in 50 mmol/L HEPES [N-(2-hydroxyethyl)piperazine-N′-(2-ethanesulfonic acid)] at pH 7 (Stookey, 1970; and Lovley and Phillips, 1986). Total Fe was determined by adding an aliquot of 10% $NH_2OH \cdot HCl$ to the sample, waiting from 4 to 24 h for complete reduction of Fe(III) to Fe(II), then measuring the color development. These determinations were made within 48 h of sampling to ensure sample integrity. The concentrations of aqueous and HCl extractable Co and Ni were determined by using ICP-AES.

The energies of ^{60}Co and ^{57}Co decay are significantly different to allow their simultaneous quantification by dual-channel counting. The activities of ^{60}Co and ^{57}Co in 1-mL aliquots of the aqueous phase and HCl extracts were determined by using a Packard Model 5000 dual-channel γ counting system (Meriden, CT, USA). The count regions for ^{60}Co and ^{57}Co were from 1050 to 1550 and from 75 to 165 keV, respectively. A correction factor was applied to the ^{57}Co data to account for the "spilldown" of ^{60}Co into the counting region of ^{57}Co.

2.8. Scanning Electron Microscopy (SEM) Analysis

Aliquots of the reduced suspensions of Co-FeOOH or Ni-FeOOH were prepared for SEM analyses under a 95% N_2 : 5% H_2 atmosphere. Two series of samples were investigated by SEM: one where samples were preserved and prepared for SEM analyses immediately after termination of the incubation period and a second where the incubated samples were allowed to age in the "spent media" for 90 days before preparation. Suspensions were filtered at 0.1 μm using Swinnex two-piece filters (Millipore, Bedford, MA, USA) and excess salts and buffers removed by three 5-mL washes with deionized distilled water (DDI). The solids were then resuspended in DDI and ~100 μL of suspension placed on carbon tape on an SEM sample stub. The sample was dried and maintained under anoxic conditions. The only exposures to air occurred during transfer from the dessicator to the gold sputter coater and then from the coater to the vacuum chamber of the scanning electron microscope.

Samples were examined by using a Model 982 field-emission scanning electron microscope (FESEM) manufactured by Leo (Helsingborg, Sweden). Morphologic analyses were performed at 5-keV accelerating potential and 90-μA filament current, utilizing the below lens detector or inlens detector, or combined below and inlens detectors. Compositional analyses by energy dispersive spectrometry (EDS) utilized a liquid nitrogen cooled Oxford Pentafet detector with the microscope operating at 20-keV potential and 90-μA current.

3. RESULTS

In the results that follow we describe the bioreduction of Co-FeOOH in six different buffer and media treatments (Table 1). Some of these contained nutrients necessary for growth, while others were deplete in either trace metals, PO_4^{3-}, or both. Each treatment contained anthraquinone disulfonate (AQDS), a quinone that functions as an electron acceptor for DIRB respiration (Scott et al., 1998) and that stimulates bacterial iron reduction (Lovley et al., 1996; Fredrickson et al., 1998; Zachara et al., 1998). AQDS was added with the belief that it would stimulate metal-goethite reduction and enhance trace-metal solubilization. In the final section of results, we present comparative data for the bioreduction of the Ni-FeOOH and also show the effects of AQDS on Co-FeOOH and Ni-FeOOH by comparison to select experiments where it was not added.

3.1. Acid Dissolution of Co-FeOOH and Ni-FeOOH

Cobalt substitutes in goethite under oxidizing conditions as the high-spin, Co^{3+} ion even when Co^{2+} was the valence form added during synthesis (Cornell and Giovanoli, 1989; Gerth, 1990), as was done here. The size mismatch between Co(III), 0.0545 nm, and Fe(III), 0.0645 nm, limits Co(III) substitution in goethite to a mole fraction of 0.1 and below (Cornell and Giovanoli, 1989; Gerth, 1990). The mole fraction of Co used in our goethite (nominally 0.01) was well below the value where exsolution and precipitation of Co(III) oxides occurs (Cornell and Giovanoli, 1989). Ni(II), with an ionic radius of 0.0690 nm, substitutes in goethite to ~5.5 mol.% (Cornell et al., 1992). Nickel concentrations above this value sorb to the oxide surface or precipitate as $Ni(OH)_2$ (Cornell et al., 1992). The synthetic

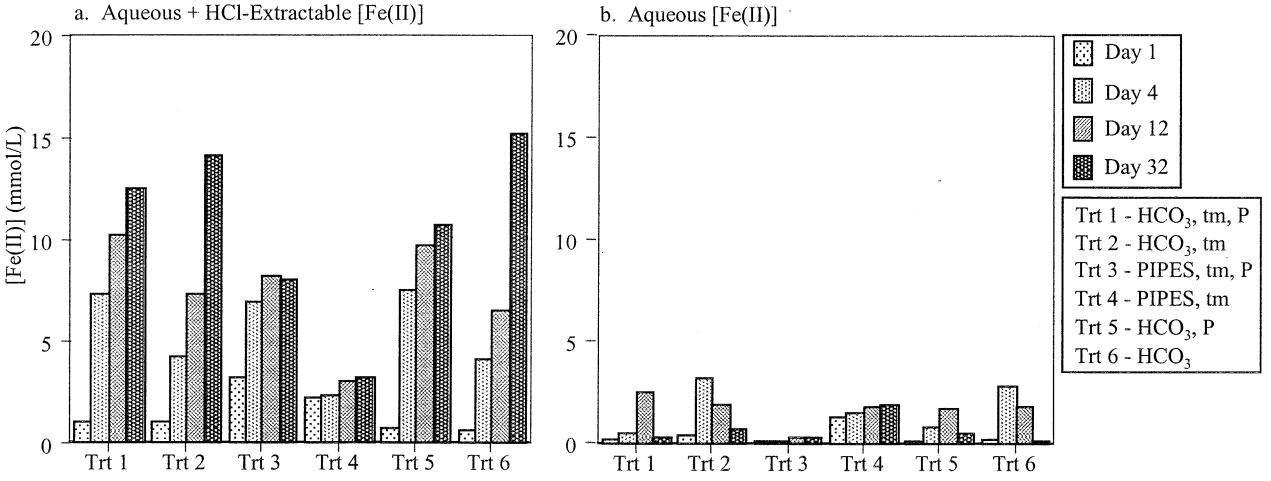

Fig. 2. HCl extractable Fe(II) (a) and aqueous Fe(II) (b) resulting from the incubation of Co-FeOOH with *S. putrefacians* in the noted buffer and media treatments.

Co-FeOOH and Ni-FeOOH existed as acicular 300-nm laths (as shown for Co-FeOOH in Fig. 1a).

The Co-FeOOH and Ni-FeOOH were dissolved to completion in HCl (Fig. 1b). The evolution of Co(III) and Ni(II) was generally congruent with Fe(III), implying that the metals were, more or less, homogeneously distributed in the goethite (Cornell and Schwertmann, 1996). The slight bowing in the dissolution curves indicated minor enrichment of Co(III) in goethite interior and minor enrichment of Ni(II) in the crystallite exterior. The congruent dissolution of Co from both substituted goethite and hematite was reported by Lim–Nunez and Gilkes (1987) and Giovanoli and Cornell (1992), while Giovanoli and Cornell (1992) showed the incongruent release of Ni from goethite in fashion consistent with its enrichment in the outer layers of the goethite.

3.2. Microbiologic Reduction of Co-FeOOH

S. putrefaciens reduced from 7.2% (media 4) to 28.8% (media 6) of the Fe(III) in Co-substituted goethite over the 32-day incubation period (Fig. 2a). The analysis of a 3.0 M HCl extraction of the bioreduced solids (e.g., Fig. 2a) was used as a measure of the total amount of Fe(II) generated [or Fe(III) reduced] at each time point (Fredrickson et al., 1998; Zachara et al., 1998). Fe(III) reduction was buffer and media dependent with the greatest amount observed in the bicarbonate buffered treatments (1, 2, 5, and 6). The evolution of Fe(II) increased with time as microorganisms metabolized lactate and transferred electrons to goethite. Phosphate enhanced the reduction rate [e.g., the amount of Fe(II) generated after Days 4 and 12] but did not necessarily effect the total amount of Fe(III) reduced after 32-day incubation. Media Treatments 1 and 3 contained the full complement of nutrients (e-donor, N, P, and trace metals) required to support growth; these treatments, however, did not lead to enhanced Fe(III) reduction over non-growth supporting regimes (e.g., Treatments 2, 4, 5, and 6).

Approximately 20 to 60% of the reduced Fe(III) was liberated to the aqueous phase as $Fe^{2+}_{(aq)}$ (Fig. 2b). The remaining biogenic Fe(II) associated with the residual Fe(III) oxide (i.e., the filterable solids) as an adsorbed or precipitated phase. In bicarbonate buffer (media Treatments 1, 2, 5, and 6), $Fe^{2+}_{(aq)}$ increased until Day 4 or 12, where approximate values of 2.5 mmol/L were reached, and then decreased to approximate values of 0.5 mmol/L (Fig. 2b). This pattern of decrease was consistent with precipitation of ferrous-iron containing solids. Aqueous Fe^{2+}, in contrast, increased with time in PIPES buffer (media Treatments 3 and 4). Media Treatment 4 in PIPES buffer had the lowest total amount of Fe(III) reduction, but the highest final concentration of $Fe^{2+}_{(aq)}$. Treatment 4 was also unusual in that 50 to 75% of the biogenic Fe(II) was released to the aqueous phase.

Microbial reduction of the Co-FeOOH lead to an increase in the suspension pH at experiment termination in spite of the presence of buffer (Table 2).

3.3. Cobalt Evolution with Microbiologic Reduction of Co-FeOOH

The evolution of both total and aqueous Co (Figs. 3a,c) closely paralleled that observed for Fe(II) (Fig. 2). Co(III) is insoluble as an oxyhydroxide (CoOOH; Hem et al., 1985) in absence of complexants (e.g., EDTA; McArdell et al., 1998), and ion chromatographic analyses of both the aqueous phase and HCl extraction from the bioreduction experiments showed Co to be present as Co(II). In media treatments 1 through 4 that contained trace metals, cobalt as a micronutrient in the medium was labeled with ^{60}Co to allow its discrimination from oxide-entrained Co(III) that was labeled with ^{57}Co. As shown in Fig. 3b and c, $Co^{2+}_{(aq)}$ was dominated by ^{57}Co that was solubilized from the Fe(III) oxide. More will be said of the ^{57}Co and ^{60}Co data in the next subsection. The enhanced rate of Fe(II) evolution observed in the presence of PO^{3-}_4, and the decrease in $Fe^{2+}_{(aq)}$ with incubation time in bicarbonate buffer as discussed above, were noted also for Co. The only difference between Co(II) and Fe(II) evolution was observed in Treatments 3 and 4 (note, Figs. 2a and 3a), where proportionally more Co was extracted by 0.5 N HCl in Treatment 4.

An operational hypothesis was that oxide entrained metals

Table 2. pH and HCO_3^- after 32-day incubation of CN32 with Co-FeOOH.

Treatment	pH		$HCO_{3(aq)}$		ΔHCO_3[a]
	Control	Biotic	Control	Biotic	
			(mol/L)		(mol/L)
1	6.9	7.4	2.17×10^{-2}	2.92×10^{-2}	$+7.50 \times 10^{-3}$
2	7.0	7.3	2.27×10^{-2}	2.32×10^{-2}	$+5.00 \times 10^{-4}$
3	7.0	7.8	2.26×10^{-4}	2.28×10^{-3}	$+2.05 \times 10^{-3}$
4	7.2	7.3	1.93×10^{-4}	1.60×10^{-3}	$+1.60 \times 10^{-3}$
5	6.9	7.3	2.15×10^{-2}	2.91×10^{-2}	$+7.60 \times 10^{-3}$
6	6.8	7.4	1.71×10^{-2}	1.75×10^{-2}	$+4.00 \times 10^{-4}$

[a] $[HCO_3^-]_{boitic} - [HCO_3^-]_{control}$.

would be liberated during bioreduction at concentrations equal to their mole fraction substitution for Fe(III). This hypothesis was qualitatively affirmed for the total Fe(II) and Co(II) pool extracted by HCl (Fig. 4a). Data from the media treatments with PO_4^{3-} (1, 3, 4, and 5) followed the 1 : 1 relationship (e.g., a ratio of Fe/Co release of 100 : 1) almost exactly, whereas those without PO_4^{3-} (2, 6) were displaced slightly to the right implying enhanced reduction of Co(III) relative to Fe(III).

The aqueous Co data, however, showed greater deviations from the expected 100[Fe(II)] : 1[Co(II)] ratio (Fig. 4b). Most of the aqueous data was displaced left of the 1 : 100 line in Figure 4b, indicating enhanced release of Co(II) relative to Fe(II). The treatments that were most distinctive in this regard (1, 2, and 3) all contained micronutrients. There was concentration dependency to the data that was difficult to generalize. Deviations from the expected 1 : 100 release ratio, whether positive or negative, were greatest at low aqueous concentrations. At higher aqueous concentrations the data converged on the 1 : 100 relationship.

3.4. Comparative Behavior of Nutrient and Solid-Phase Co

The nutrient (traced by ^{60}Co) and solid-phase Co(II) (traced by ^{57}Co) showed markedly different behavior with bioreduction (Fig. 5, representing an integration of data from Fig. 3). The nutrient Co(II) [at 10^{-6} mol/L] was added in mixture with NTA (Table 1). Speciation calculations of the nutrient solutions for treatments 1 through 4 using the best available thermodynamic data indicated that the initial degree of Co(II) complexation by NTA was 99.6% in bicarbonate buffer and 99.7% in PIPES buffer. In spite of this complexation, nutrient Co(II) was initially adsorbed by the oxide, lowering its aqueous concentration to $\sim 10^{-6.4}$ mol/L in all treatments. With bioreduction, most of the adsorbed nutrient Co(II) was released back to the aqueous phase (Fig. 5). There were subtle differences in sorption between media treatments, with greater initial and final adsorption noted in the absence of PO_4^{3-} (Treatments 2 and 4). With bioreduction of Co-FeOOH, the concentrations of oxide-derived Co(II) as traced by ^{57}Co increased in both the aqueous

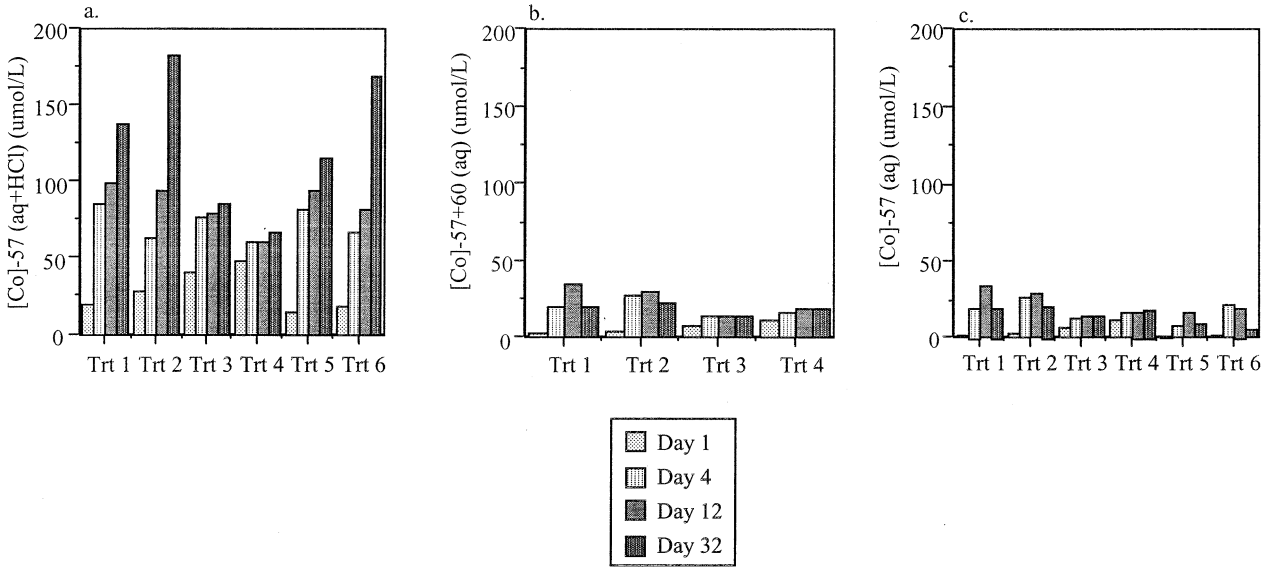

Fig. 3. HCl extractable solid-phase Co(II) (^{57}Co) (a), aqueous phase ^{57}Co(II) (b), and total aqueous Co(II) ($^{57}Co + {}^{60}Co$) (c) resulting from the incubation of Co-FeOOH with *S. putrefacians* in the noted buffer and media treatments.

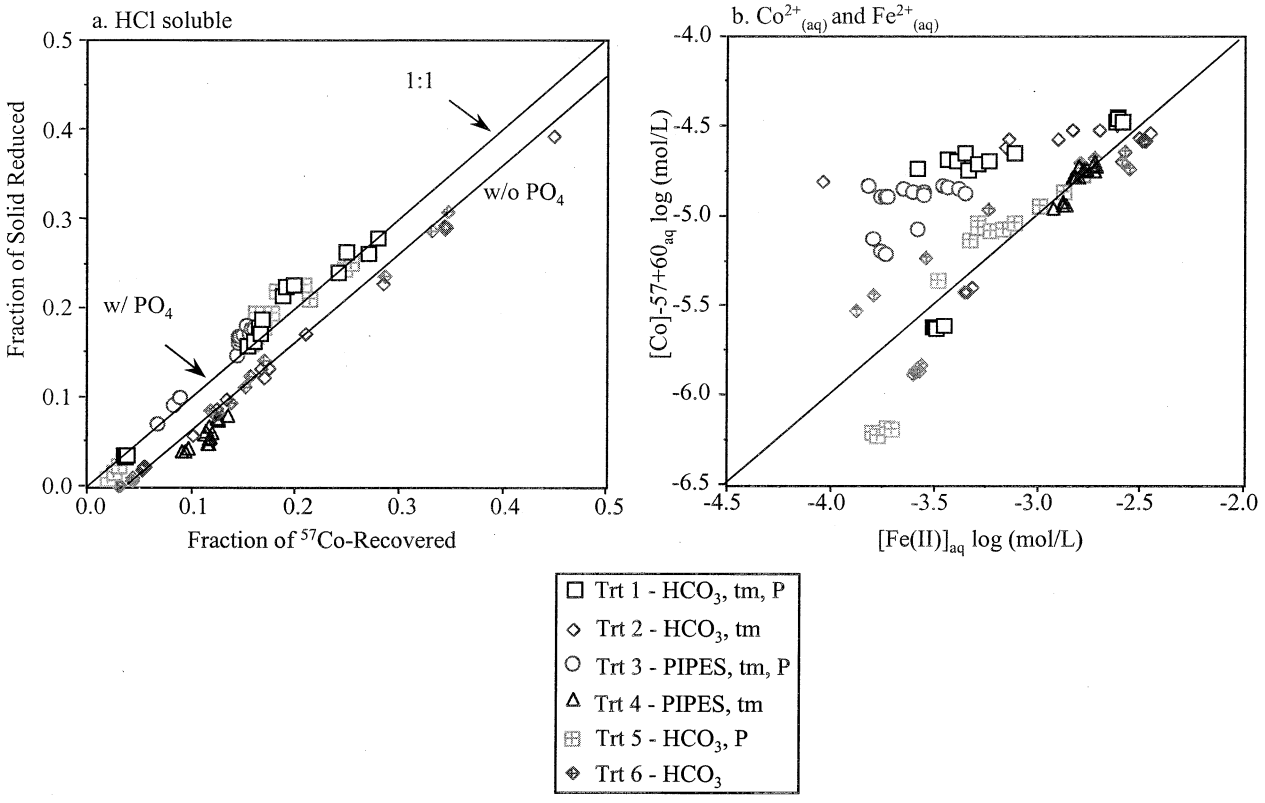

Fig. 4. Relationships between fraction of Co-FeOOH reduced and fraction of Co(III) recovered as Co(II) by HCl extract (a), and the total aqueous Co(II) and Fe(II) concentrations (b). Solid lines in both panels represent a 100:1, Fe(II) to Co(II) ratio.

phase and the HCl extractable (sorbed) pool by 1.5 orders of magnitude or more (Fig. 5). With continued bioreduction, the aqueous Co(II) concentrations increased to a threshold value of $\sim 10^{-4.75}$ to $10^{-4.3}$ mol/L, and then began to decrease for treatments in bicarbonate buffer (1, 2, 5, and 6).

Concentration distribution ratios, K_d (where $K_d = \{[Co(II)_{HCl} - Co(II)_{aq}]/[Co(II)_{aq}]\}$ in L/g), were computed for each media treatment and time point to further distinguish between the biogeochemical behavior of the two Co(II) pools (Fig. 6). The K_d embodies no assumption about the reversibility

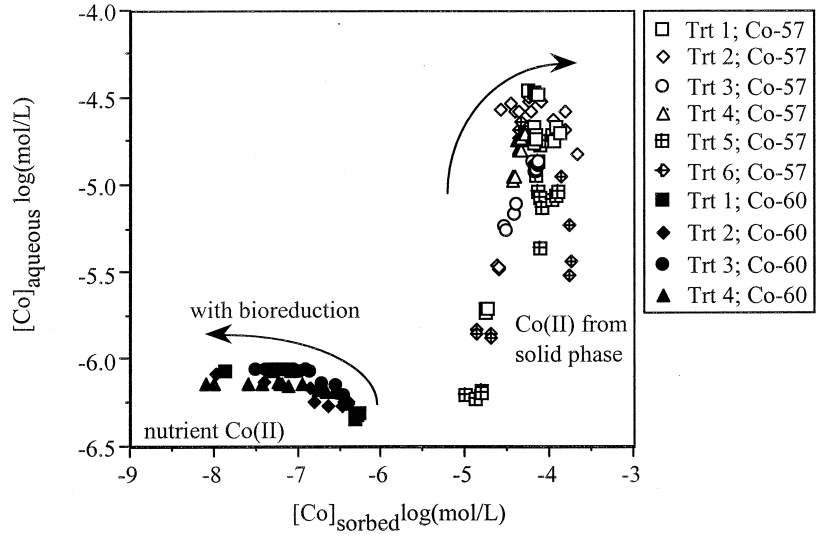

Fig. 5. The nutrient (^{60}Co) and solid-phase (^{57}Co) Co pools were distinct and showed different behavior with bioreduction. Only four of the media treatments contained nutrient Co(II).

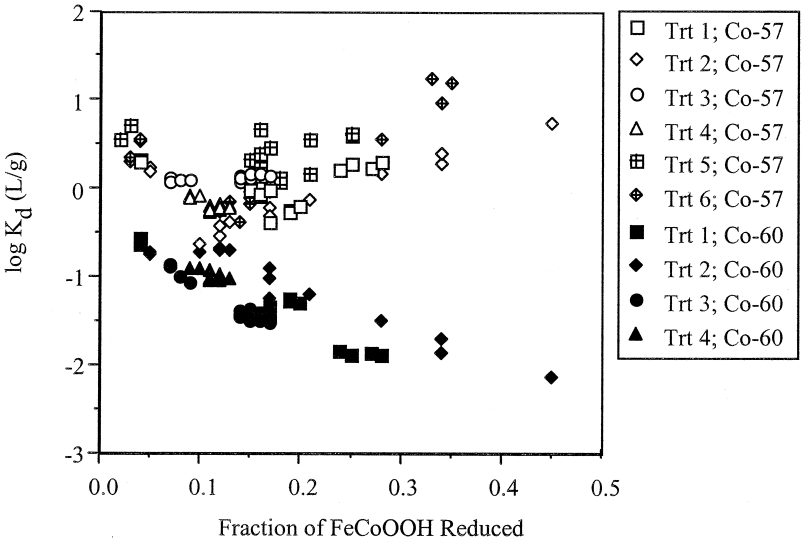

Fig. 6. Solid-liquid distribution of nutrient (^{60}Co) and solid-phase (^{57}Co) Co pools during the course of Co-FeOOH reduction as measured by a concentration-distribution ratio [K_d (L/g)].

or chemical nature of the sorption complex {e.g., [$Co(II)_{HCl}$ − $Co(II)_{aq}$]}, which may be an adsorbed species or a precipitate. The K_d values fell into distinct groupings for both the nutrient- and oxide-entrained Co (Fig. 6). Nutrient Co(II) was consistently less strongly sorbed than was Co(II) originating from reduction of Co(III) in the oxide. K_d values for nutrient Co(II) decreased with fractional reduction of the solid consistent with Figure 5. Below a fractional reduction of 0.15 (15% of solid reduced), K_d values for solid-phase Co(II) paralleled those for nutrient Co(II) in decreasing trend, but were elevated by an order of magnitude or more. The K_d values increased above 0.15 and showed scatter and variation between media treatments, possibly as a result of discrete [e.g., Co(II) alone] or mixed phase [e.g., with Fe(II)] precipitation.

3.5. Formation of Fe(II) Solid Phases

X-ray diffraction and SEM was applied to the residual mineral solids at experiment termination (32 days) to identify biomineralization products. Vivianite [$Fe_3(PO_4)_2 \cdot 8H_2O$] was observed in all treatments containing PO_4^{3-} in both buffer systems (1, 3, and 5). It was clearly identified by X-ray diffraction (Fig. 7a) and by its distinctive pinnacoid, bladed and, occasionally, fibrous, morphology (Fig. 7b). The vivianite crystallites ranged between 5 to 30 μm (Fig. 7b), were often intergrown and aggregated, and were considerably larger than the goethite laths (ca., 400 nm, Fig. 1) or CN32 cells (ca., 1.5 μm, not shown). Siderite ($FeCO_3$) was observed in all media treatments containing bicarbonate buffer. It was clearly distin-

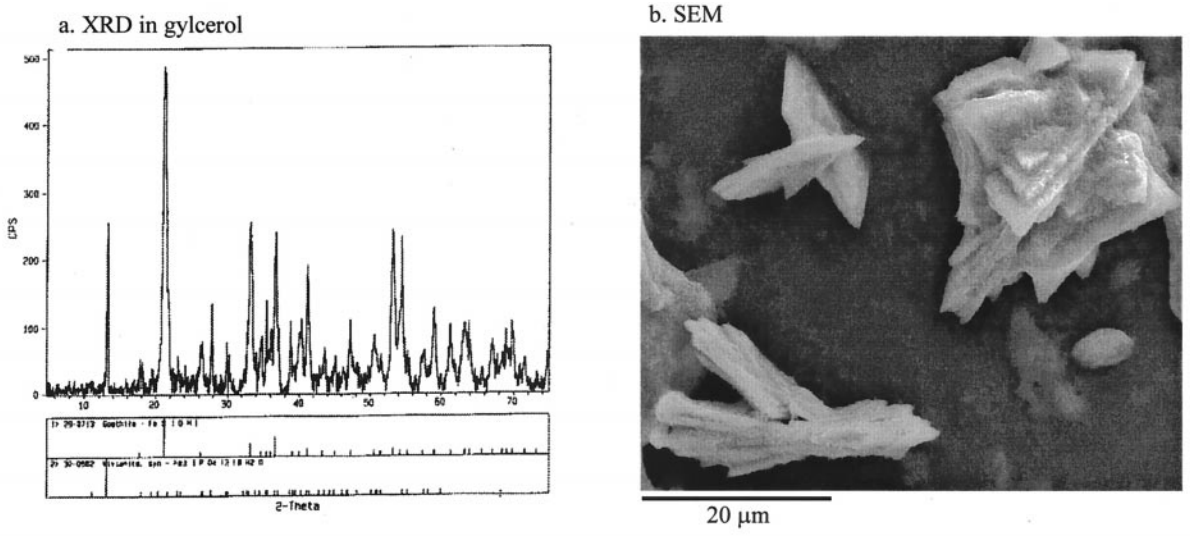

Fig. 7. Vivianite [$Fe_3(PO_4)_2 \cdot 8H_2O$] precipitates in bioreduced Co-FeOOH suspensions in PIPES buffer containing PO_4 after 32 d incubation. X-ray diffraction (a) and electron micrograph (b).

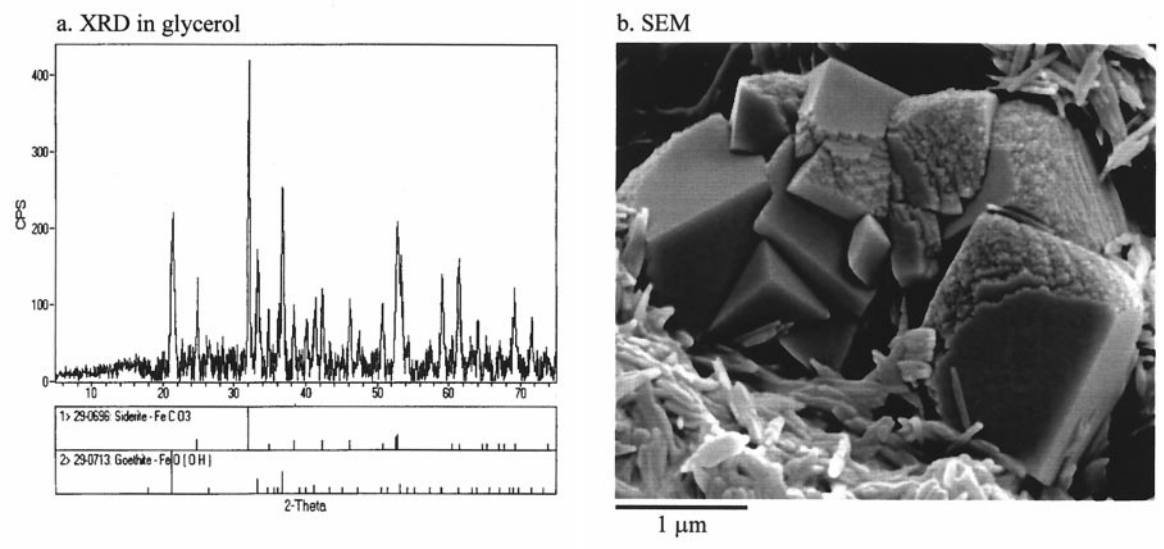

Fig. 8. Siderite ($FeCO_3$) precipitates in bioreduced Co-FeOOH suspensions in bicarbonate buffer after 32-day incubation. X-ray diffraction (a) and electron micrograph (b).

guished by X-ray diffraction (Fig. 8a) and by its rhombohedral morphology (Fig. 8b). The crystallites were approximately 1 μm on edge and were observed as single crystals dispersed in a goethite groundmass (Fig. 8b). Both vivianite and siderite were observed in media Treatments 1 and 5; siderite was often observed as small rhoms apparently attached to vivianite (Fig. 9). Semi-quantitative mass determinations from XRD peak heights yielded 50% goethite, 30% vivianite, and 20% siderite for Treatment 1 (data not shown). Media 4 (PIPES buffer without PO_4^{3-}) was the only treatment where secondary ferrous precipitates were not observed by X-ray diffraction or SEM.

The aqueous concentrations of HCO_3^- and PO_4^{3-} at experiment termination (Tables 2 and 3) provided evidence for mass loss by precipitation. Presumptive evidence for the timing of vivianite precipitation was provided by the behavior of aqueous P (Table 3) which decreased by ~95%, relative to uninoculated controls, in the first 4 to 12 days of incubation. This rapid P removal implied that vivianite quickly formed by reaction of biogenic Fe(II) with nutrient P. However, we cannot discount P consumption by the cells as it would likely have occurred over this same time frame. Bicarbonate was liberated from the metabolism of lactate in an approximate ratio of HCO_3 : Fe(II)

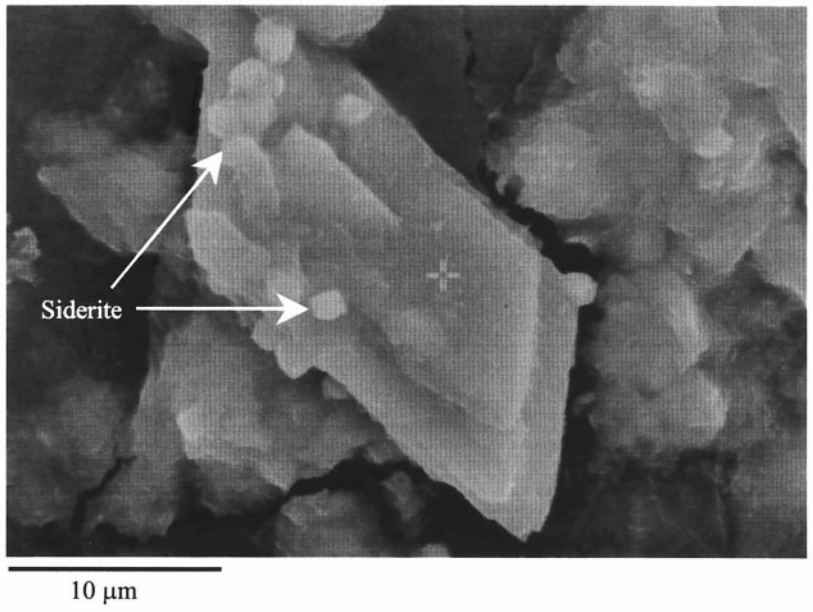

Fig. 9. Intergrown siderite and vivianite precipitates in bioreduced Co-FeOOH suspensions in bicarbonate buffer with PO_4.

Table 3. Phosphate concentrations in reduction experiments and controls.

Day	Treatment 1		Treatment 3		Treatment 5	
	Control[a]	Biotic[b]	Control[a]	Biotic[b]	Control[a]	Biotic[b]
	(mol/L)					
1	3.65×10^{-3}	3.36×10^{-3}	3.52×10^{-3}	2.03×10^{-3}	3.47×10^{-3}	3.58×10^{-3}
4	3.62×10^{-3}	7.23×10^{-5}	3.44×10^{-3}	1.00×10^{-4}	3.53×10^{-3}	1.60×10^{-4}
12	3.58×10^{-3}	$<2.6 \times 10^{-5}$	3.55×10^{-3}	$<1.48 \times 10^{-5}$	3.51×10^{-3}	$<2.61 \times 10^{-5}$
32	3.55×10^{-3}	$<2.6 \times 10^{-5}$	3.49×10^{-3}	$<1.48 \times 10^{-5}$	3.50×10^{-3}	$<1.47 \times 10^{-5}$

[a] Mean of two replicates.
[b] Mean of four replicates.

of 1 : 4 (Zachara et al., 1998). Evidence for HCO_3^- evolution was observed in the PIPES buffered Treatments (3 and 4) and the bicarbonate buffered treatments with P (1 and 5; Table 2) where significant net accumulation was observed. In contrast, HCO_3^- did not appreciably accumulate in the media without P (Table 2) because of its apparent incorporation in $FeCO_3$. These observations implied that P retards the initial precipitation of $FeCO_3$ by competition or surface poisoning, and are consistent with a thermodynamic model proposed by Zachara et al. (1998), where the less soluble vivianite precipitates to completion before the onset of siderite precipitation.

Saturation indicies were computed for siderite, vivianite, and select cobalt phases (hydroxides, carbonate, phosphate) at experiment termination (Table 4) based on the concentration of added nutrients (Table 1), the measured solution composition (Appendix Table 1), and the pH. The saturation index (S.I., Table 4) defines whether a solution is oversaturated (log S.I. $>$ 0), undersaturated (log S.I. $<$ 0), or in equilibrium (log S.I. $=$ 0) with the tested mineral phase. Lactate and acetate were not directly measured, but their concentrations were estimated from the stoichiometric relationship with Fe(II) as reported by Zachara et al., (1998). The S.I. calculations included the effects of aqueous complexation by acetate, lactate, carbonate/bicarbonate, phosphate, and NTA where appropriate. The accuracy of the computed S.I. values are dependent on analytic precision (e.g., total inorganic C and total phosphate) and the quality of the thermodynamic data, which is limited for the Co(II) solids.

The ferrous containing solids [$FeCO_3$, $Fe_3(PO_4)_2 \cdot 8H_2O$] were typically computed to be supersaturated, indicating thermodynamic driving force for precipitation. Supersaturation was consistent with the presence of these phases (Figs. 7–9). Their supersaturation indicated that the rate of biotic Fe(II) generation exceeded the precipitation rate, or alternatively, that the free energy of the biotically precipitated solids differed from the abiotic ones used for S.I. calculation (e.g., Bruno et al., 1992; Al-Borno and Tomson, 1994). In contrast, the Co(II) solids were generally undersaturated, implying that the formation of discrete Co(II)-hydroxide, carbonate, or phosphate solids was unlikely. We did note that the morphology of the bioreduced material in bicarbonate buffer changed markedly with aging (Fig. 10); with the residual mineral material becoming encrusted or enabulated with further $FeCO_3$ precipitate (determined by EDS analysis, not shown). This may have resulted from the relief of siderite supersaturation by slow precipitation, continued biotic Fe(II) generation, or both. Generally, the computed effects of lactate and acetate on Fe(II) or Co(II) speciation were minimal because of the small values of their respective complexation constants (e.g., log K values at 25°C and I = 0 range between 1 and 2; Smith and Martell, 1997).

A coprecipitation experiment was performed to assess the relative ability of Co(II) to substitute in vivianite, believing that such a reaction could be important to the post reduction distribution of Co in experiments with media phosphate. The exper-

Table 4. Saturation indicies after 32-day incubation of Co-FeOOH with CN32.

Treatment	Saturation index[a]				
	$FeCO_{3(s)}$[b]	$Fe_3(PO_4)_3 \cdot 8H_2O$[c]	$Co(OH)_2$[d]	$Co_3(PO_4)_2 \cdot 8H_2O$[e]	$CoCO_3$[f]
1	1.68	3.51	−4.55 to −3.16	−1.89	−0.091
2	1.86	NA[g]	−5.71 to −4.32	NA	−1.16
3	1.22	4.08	−3.64 to −2.84	−1.68	−0.67
4	1.25	NA	−4.46 to −3.06	NA	−1.18
5	1.72	2.76	−5.14 to −3.75	−4.22	−0.58
6	1.25	NA	−4.99 to −3.61	NA	−0.75

[a] Computed with MINTEQA2 (Allison et al., 1991). Saturation index = log $IAP_{(exp)}/IAP_{(equil)}$ where $IAP_{(exp)}$ is the experimental ion activity product for the given phase and $IAP_{(equil)}$ is the ion activity product at equilibrium.
[b] Bruno et al. (1992).
[c] Al-Borno and Tomson (1994).
[d] Naumov et al. (1974) for transvaalite.
[e] Rudii and Antraptseva (1991).
[f] Naumov et al. (1974) for sphaerocobaltite.
[g] NA, not applicable; PO_4^{3-} was not in the medium.

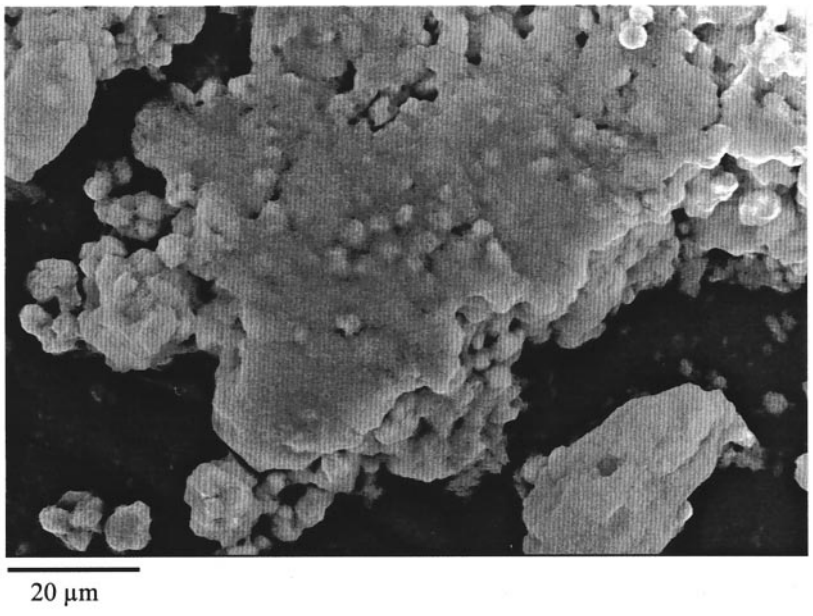

Fig. 10. Siderite entabulation of bioreduced Co-FeOOH in bicarbonate buffer after 90 days aging in "spent media."

iment was performed by precipitating vivianite, in the presence of dilute Co(II) [e.g., Fe : Co = 100] according to the procedure of Al-Borno and Tomson (1994). The procedure precipitated 99.8% of the Fe(II) and 98.8% of the Co(II), and the product yielded a well-defined X-ray diffractogram of vivianite, without apparent mineralogic impurities. We assumed, but did not experimentally document, that Co(II) was homogeneously coprecipitated in vivianite. A conditional equilibrium constant (K_c) or separation factor (D; Sposito, 1981) was computed for the following exchange reaction after analyzing the solution and solid after 2 months aging.

$$Fe_3(PO_4)_2 \cdot 8H_2O + 3Co^{2+} = Co_3(PO_4)_2 \cdot 8H_2O + 3Fe^{2+} \qquad K_c/D$$

Where $D = (N_{Co})(Fe^{2+})^3/(N_{Fe})(Co^{2+})^3$, and N_{Co} and N_{Fe} are mole fractions of the components in the coprecipitate. The computed value of D was 8.73, indicating significant tendency for Co(II) to coprecipitate in vivianite at the concentrations used.

3.6. Relative Behavior of Ni-FeOOH and Co-FeOOH

A comparative study was performed with CN32 on the effects of AQDS on metal solubilization from both Co-FeOOH and Ni-FeOOH. Eight treatments were compared for both the Co-FeOOH and Ni-FeOOH (all without trace nutrient supplement): PIPES buffer with and without PO_4^{3-} and with and without AQDS, and bicarbonate buffer with and without PO_4^{3-} and with and without AQDS (Table 5). The same batch of Co-FeOOH was used for these as in the preceding experiments. These media treatments were sampled only once with the objective of comparing the final state after a 25-day period of bioreduction.

The CN32 culture used in these later experiments reduced smaller amounts of Fe(III) oxide (3.5–18.4%, Table 5) then observed previously in the Figure 2 experiments. We have previously noticed and reported on such variations in reduction by CN32 with HFO (Fredrickson et al., 1998). The smaller amount of reduction possibly resulted from the shorter incubation time used in the latter experiment (25 days as compared to 32 days). Consequently, there was difference between media treatments that did and did not contain PO_4^{3-} (Table 5). The earlier studies showed that the rate of bioreduction [e.g., Fe(II) evolution, Fig. 2] was faster when PO_4^{3-} was present, and consistent with that, the later study showed that PO_4^{3-} yielded a greater amount of reduction after 25 days (Table 5). Unlike previously reported studies with crystalline Fe(III) oxides (Zachara et al., 1998), AQDS did not significantly enhance the extent of reduction of either Co-FeOOH or Ni-FeOOH.

The Co-FeOOH and Ni-FeOOH behaved almost identically during bioreduction (Table 5). The Ni-FeOOH showed slightly less reduction and more metal release to HCl extraction than the Co-FeOOH, but all other trends with respect to media components and buffer were the same. The solid residues from incubations of both the Co-FeOOH and Ni-FeOOH were examined by both XRD and SEM, and these showed no differences from one another. Vivianite and siderite were again observed as biomineralization products at relative concentrations consistent with total extent of Fe(III) oxide reduction. No distinct solid phases or morphologic changes to vivianite or siderite were observed in the bioreduced Ni-FeOOH.

4. DISCUSSION

4.1. Thermodynamics of Reduction

S. putrefaciens strain CN32 has been shown previously to couple the oxidation of lactate with the reduction of various poorly crystalline and crystalline Fe(III) oxides (Fredrickson et al., 1999; Zachara et al., 1999). Here we have seen that lactate-driven bioreduction of goethite can mobilize, in part, minor

Table 5. The effect of AQDS on the bioreduction and solubilization of metals from Co-FeOOH and Ni-FeOOH after 25 days of incubation.

	FeCoOOH											
	With AQDS						Without AQDS					
Media components	Aqueous [Fe] (mmol/L)	Extractable Fe (mmol/L)	Aqueous Co (mmol/L)	Extractable Co (mmol/L)	Extr Fe:Co (mol/mol)	% of Solid Reduced	Aqueous [Fe] (mmol/L)	Extractable Fe (mmol/L)	Aqueous Co (mmol/L)	Extractable Co (mmol/L)	Extr Fe:Co (mol/mol)	% of Solid Reduced
PIPES with phosphate	0.36	7.43	0.004	0.060	123	14.6	0.76	7.70	0.009	0.065	118	15.1
PIPES without phosphate	1.88	3.04	0.016	0.031	97	6.0	1.71	2.42	0.014	0.025	98	4.7
HCO_3 with phosphate	1.93	9.40	0.020	0.080	118	18.4	1.02	7.79	0.012	0.067	116	15.3
HCO_3 without phosphate	3.52	4.92	0.029	0.053	94	9.7	2.48	3.58	0.023	0.041	88	7.0
	FeNiOOH											
	With AQDS						Without AQDS					
Media components	Aqueous [Fe] (mmol/L)	Extractable Fe (mmol/L)	Aqueous Ni (mmol/L)	Extractable Ni (mmol/L)	Extr Fe:Ni (mol/mol)	% of Solid Reduced	Aqueous [Fe] (mmol/L)	Extractable Fe (mmol/L)	Aqueous Ni (mmol/L)	Extractable Ni (mmol/L)	Extr Fe:Ni (mol/mol)	% of Solid Reduced
PIPES with phosphate	0.20	6.71	0.010	0.094	72	13.2	0.18	6.27	0.010	0.094	67	12.3
PIPES without phosphate	1.41	2.42	0.011	0.036	68	4.7	1.24	1.79	0.015	0.035	51	3.5
HCO_3 with phosphate	1.19	8.24	0.027	0.11	74	16.1	0.24	6.27	0.012	0.090	67	12.3
HCO_3 without phosphate	3.17	4.57	0.023	0.060	77	9.0	2.05	2.95	0.017	0.046	64	5.8

Table 6. Reduction potentials of lactate (L^-) and anthraquinone disulfonate (AQDS) relative to Fe(III) and Co(III) oxides.

Half-reaction	$E°$[a] (Volts)	E'[b] (Volts)	Source
1. $CoOOH_{(s)} + 3H^- + e^- = Co^{2+} + 2H_2O$	+1.48	+1.59	Stone and Ulrich, 1989
2. $FeOOH + 1.67H^+ + 0.67H_2PO_4^- + 2.67H_2O + e^- = 0.33Fe_3(PO_4)_2 \cdot 8H_2O$	0.793	0.011[c]	Cornell and Schwertman, 1996 Al-Borno and Tomson, 1994
3. $FeOOH_{(s)} + HCO_3^- + 2H^+ + e^- = FeCO_{3(s)} + 2H_2O$	0.848	−0.070[d]	Cornell and Schwertman, 1996 Bruno et al., 1992
4. $FeOOH_{(s)} + 3H^- + e^- = Fe^{2+} + 2H_2O$	+0.67	−0.22	Stone and Ulrich, 1989
5. $0.5AQDS + H^- + e^- = 0.5AHDS$	+0.23	−0.24	Clark, 1960
6. $0.125A^- + 0.25HCO_3^- + 1.2H^+ + e^- = 0.166L^- + 5H_2O$[5]	+0.121	−0.396 (HCO_3^- buffer) −0.410 (PIPES buffer)	

[a] $E°$ = standard reduction potential.
[b] E' = reduction potential with $[H^+] = 1.0 \times 10^{-7}$ mol/L, $[Me^{2+}] = 1.0 \times 10^{-6}$ mol/L, [AQDS] = 1.0×10^{-6} mol/L and [AHDS] = 1.0×10^{-4} mol/L.
[c] $H_2PO_4^-$ = 4.0 mM.
[d] HCO_3^- = 30 mM.
[e] A^- = acetate (CH_3COO^-); L^- = lactate ($CH_3CHOHCOO^-$).

elements that are coprecipitated within the bulk structure of FeOOH.

An effective free energy ladder for redox-sensitive species in our experimental system is shown in Table 6. Effective redox potentials (E') are summarized that were derived from standard state potentials ($E°$) by using the Nernst equation. Reduction reactions leading to ferrous iron solid-phase products [e.g., $FeCO_3$, $Fe_3(PO_4)_2 \cdot 8H_2O$] are included as these were shown to occur and their explicit inclusion is necessary for proper thermodynamic analysis. Lactate exhibits the lowest effective redox potential (E') and, through microbial mediation, drives the reduction of the other couples. The strongest oxidant is the $CoOOH/Co^{2+}$ couple which yields the largest free energy change in reaction with lactate. Baring kinetic constraints, it should be the first to react with electrons liberated by bacterial lactate oxidation. Cobalt(III) is susceptible to reduction by DIRB when present in aqueous complex [e.g., Co(III)EDTA; Gorby et al., 1998]; and our measurements indicate that it is either directly (enzymatically) or indirectly [by Fe(II)] reduced in Co-FeOOH. Co(II) was the observed valence form in both the aqueous phase and the HCl extract.

The amount of Co-FeOOH reduction in bicarbonate buffer was from 30 to 50% greater than observed in PIPES buffer (Fig. 2). This observation is consistent with the E' values in Table 6, if it is assumed that Reactions 3 and 4 in Table 6 are dominant in bicarbonate and PIPES buffers, respectively. The bioreduction of goethite is favored under conditions leading to siderite precipitation as a larger free-energy change is associated with this reaction. Similarly, the greater reduction observed in PIPES buffer when P was present (Fig. 2) may be rationalized, in part, as a consequence of the favorable thermodynamics of Reaction 2 driven by vivianite precipitation.

AQDS was added to many of the inoculated suspensions of Co-FeOOH and Ni-FeOOH to enhance solid-phase reduction. Previous research with both HFO, goethite, hematite, and subsurface materials containing crystalline Fe(III) oxides has shown that AQDS stimulates both the rate and extent of Fe(III) reduction (Fredrickson et al., 1998; Zachara et al., 1998). The effective redox potential (E') of the AQDS couple lies below that of FeOOH and above that of lactate (Table 6). AQDS readily accepts electrons from respiring DIRB (Lovley et al., 1996; Fredrickson et al., 1999), producing the reduced, anthrahydroquinone form (AH_2DS). The hydroquinone (AH_2DS) has marginal thermodynamic power to reduce FeOOH to $Fe^{2+}_{(aq)}$ (Reaction 4), but the free energy is sufficiently favorable to produce siderite (Reaction 3) if requisite concentrations of HCO_3^- are present.

4.2. Fate of Biogenic Fe(II)

In general, 50% or more of the biogenic Fe(II) was associated with the residual Fe(III) oxide. In media Treatments 1, 2, 5, and 6 (Table 1) with bicarbonate buffer, $Fe^{2+}_{(aq)}$ concentrations generally increased through Day 4 or 12 of incubation and then decreased (Fig. 2), consistent with mineral precipitation. In these media, siderite or a combination of siderite and vivianite were observed. Under requisite abiotic conditions, vivianite readily precipitates (Al-Borno and Tomson, 1994), but siderite is slow to form and exhibits sluggish precipitation kinetics (Greenberg and Tomson, 1992). Iron-reducing bacteria mediate siderite precipitation in mineral suspensions (Mortimer and Coleman, 1997; Fredrickson et al., 1998; Zachara et al., 1998) and sediments (Postma, 1981; Pye et al., 1990; Sawicki et al., 1995), although the manner by which microorganisms accelerate siderite precipitation is not known. Both siderite and vivianite were significantly greater in size (2–20 μm) than goethite (0.30–0.40 μm) and their dispersed nature implied their role as global Fe(II) sinks. They appeared to form from homogeneous precipitation, rather than by topo-tactic growth on goethite or bacteria surfaces. The extent and morphology of the siderite and vivianite biomineralization was comparable to that observed for the bioreduction of goethites without metal substitution (Zachara et al., 1998), implying little or no effect of evolved Ni^{2+} or Co^{2+}.

In PIPES buffer without P, biogenic Fe(II) sorbed to, and eventually saturated the residual Fe(III) oxide and bacterial cell surfaces, leading to increased $Fe^{2+}_{(aq)}$ concentrations (Treatment 4, Fig. 2). We have previously observed that dissimilatory Fe(III) reduction tends to slow or cease when the crystalline Fe(III) oxide surface becomes Fe(II) saturated (Roden and

Zachara, 1996). Complexants or ligands that promote the formation of aqueous Fe(II) complexes or solid phases, in turn, may enhance bacterial Fe(III) oxide reduction by drawing Fe(II) from the residual Fe(III) oxide surface (Urrutia et al., 1998). The extent of Fe(III) reduction observed with the Me-FeOOH (Fig. 2) was consistent with previous observations; the least reduction occurred in Treatment 4, where there was no evidence for secondary phase formation. The surface chemical nature of sorbed Fe(II) is not well known and is difficult to interrogate spectroscopically. Haderlein and Pecher (1999) used the surface precipitation model of Farley et al., (1985) to fit Fe(II) sorption data on goethite in the circumneutral pH range [with $Fe(OH)_2$ as the surface precipitating phase] and proposed that surface clusters and precipitates dominate the speciation of sorbed Fe(II) on goethite.

The biogeochemical behavior of Fe(II) is of crucial importance to the release and solubility of the evolved Co(II) both through competitive sorption on the residual oxide surface and through coprecipitation in Fe(II) solids as discussed below.

4.3. Factors Controlling Co(II) Evolution

4.3.1. Bioreduction of the Co(III) in Co-FeOOH

Co(II) appeared to be generated by CN32 in a concentration that paralleled its mole ratio in the Co-FeOOH (Fig. 4a). Similarly, Bousserrhine et al., (1999) observed the congruent reductive dissolution of a 5% Co-FeOOH by an acid producing, fermenting bacterium (*Clostridium butyricium*). Thus, in spite of the more favorable reduction thermodynamics of the Co(III)/Co(II) pair (Table 6), there was no apparent preferential reduction of Co(III) in the solid. The bioreduction process appeared consistent with a homogeneous advancing front model where electron transfer occurred in direct proportion to bulk cation concentrations. There was no evidence for deeper electron transfer into the structure to more energetically favorable Co(III) sites, as may have been anticipated from the E′ values in Table 6. These conclusions, however, are made with caution because they were based on HCl extraction of the bioreduced solid only. The dilute HCl extraction is effective in displacing Fe(II) associated with surfaces and in dissolving Fe(II) coatings and relatively soluble Fe(II) biomineralization products including siderite, vivianite, and fine grained magnetite. It dissolves little of the residual FeOOH. It is likely that deep reduction of Co(III) in Co-FeOOH could not have been discriminated by HCl extraction unless the solid was fully dissolved. We attempted to characterize Co(III/II) in the bioreduced solids by K-edge X-ray absorption spectroscopy to address this question but were unsuccessful because of the similar energies of the Fe and Co adsorption edges and the relatively low concentration of Co.

4.3.2. Solubilization of biogenic Co(II)

The release of biogenic Co(II) to the aqueous phase, (e.g., Fig. 4b) varied with media composition and buffer, but unequivocal relationships were not evident. We expected, but did not observe, that solubilization would be enhanced in bicarbonate buffer over that in PIPES buffer through carbonate complexation of Co^{2+}. For example, 63.4% of 10^{-5} mol/L Co(II) was computed to exist as $CoHCO_3^-$ in 30 mM $NaHCO_3$ buffer at pH 7 ($\log K_{CoHCO3} = 12.5$; $\log K_{CoCO3} = 4.41$), with the net contribution of bicarbonate and carbonate complexes increasing with increasing pH (e.g., note experimental pH values in Table 2). Enhanced solubilization was also not observed as acetate accumulated as a result of lactate oxidation. CN32 produces acetate in 1 : 4 ratio with Fe(II) (Zachara et al., 1998); the highest concentrations of acetate, therefore, existed in the FeCoOOH suspensions with the greatest Fe(II) generation. The acetate complexes with Fe(II), Co(II), and Ni(II) are, however, all weak, with log K values for formation ranging between 1.40 to 1.46 (Smith and Martell, 1997).

The apparent sorption strength of nutrient (^{60}Co) and biogenic (^{57}Co) Co(II) [as measured by K_d, Fig. 6] were different from one another. Biogenic Co(II) was sorbed more strongly. Although nutrient Co(II) was computed to be complexed by NTA added with the trace metals solution, Girvin et al. (1996) noted that hydroxyl surface sites on metal oxides are able to outcompete NTA for Co(II). Such competition was likely in our system, especially since there were other metal cations [nutrients and Fe(II)] that would have enhanced dissociation of $CoNTA^-$. The results presented in Figure 6 implied that the chemical environment of biogenic Co(II) on the reduced goethite surface was different from that of a Co(II) surface complex that formed on the same surface under identical aqueous conditions.

The data in Figure 6 for biogenic Co(II) (mol/g sorbed) was replotted and compared to an abiotic adsorption isotherm measured for $Co^{2+}_{(aq)}$ at pH 7.3 in PIPES buffer (Fig. 11a). A subset of the biogenic Co(II) data paralleled the isotherm but was elevated above it (more strongly sorbed) by ~0.75 orders of magnitude. This data, which is assumed to represent the adsorbed Co(II) fraction, was the same subset observed in Figure 6 below a reduced fraction of 0.15. The data cluster that exists above the biogenic Co(II) isotherm in Figure 11a and above a reduced fraction of 0.15 in Figure 6 was believed to represent a precipitated Co(II) fraction that was incorporated within biogenic ferrous solids.

Adsorption. Adsorbed biogenic Co(II) was more strongly bound to the residual Fe(III) oxide surface than was Co^{2+} adsorbed from the aqueous phase on either the pristine or bioreduced surface. Our working hypothesis was that biogenic Co(II) would be solubilized from the residual Fe(III) oxide by strong competitive mass action from biogenic Fe(II) and that the resulting biogenic Co(II) isotherm would be lower than that observed for the pristine Co^{2+}/goethite system (Fig. 11a). This working hypothesis was based on comparative sorption measurements of both Fe^{2+} and Co^{2+} as individual solutes on this same goethite under anoxic conditions in the absence of bioreduction (Zachara et al., 1999), and the observation that excess Fe^{2+} (e.g., 200 : 1) inhibits Co^{2+} adsorption (Fig. 11b).

In a previous study (Zachara et al., 2000), we attempted to determine whether sorbed Fe(II) on goethite arising from bacterial reduction followed the same isotherm as did Fe(II) spiked to a microbe-free, anoxic goethite suspension (abiotic isotherm). While the study was not unequivocal, the results indicated that, similar to those for Co(II) above, biogenic Fe(II) exhibited a higher preference isotherm than did abiotically spiked Fe(II). The abiotic and biogenic isotherms were generated and measured differently. In the abiotic system, known concentrations of Fe(II) were spiked to the aqueous phase and the concentration difference after equilibration was used to

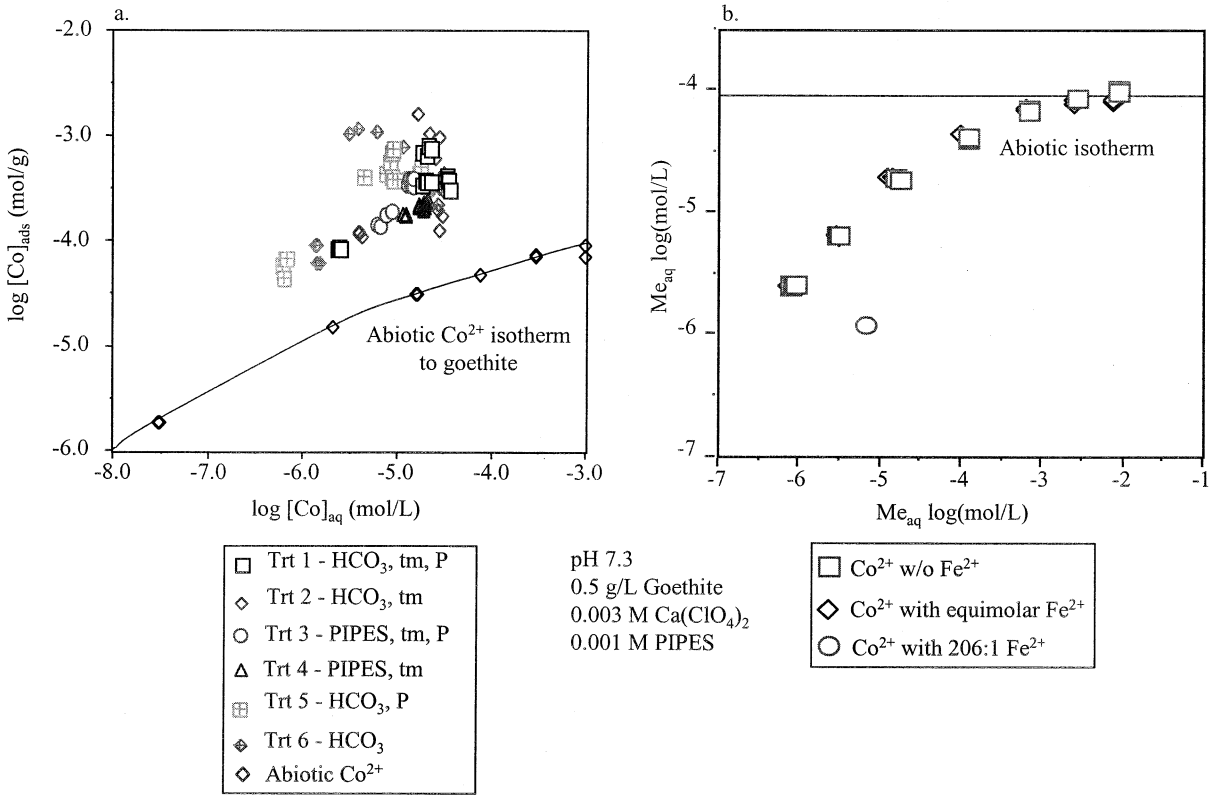

Fig. 11. (a) "Adsorption isotherm" of Co(II) from the bioreduction experiment compared to an abiotic adsorption isotherm of $Co^{2+}_{(aq)}$ measured on the starting goethite under anoxic conditions. The sorbed concentrations of Co(II) from the bioreduction experiment were defined as those obtained by HCl extraction minus the total aqueous Co(II) concentration. (b) Competitive isotherm for $Co^{2+}_{(aq)}$ on the starting goethite under anoxic conditions with equimolar Fe(II) and excess Fe(II) (one point only to avoid precipitation effects).

calculate the adsorption density. The isotherm that resulted is a plot of adsorbed concentration versus aqueous concentration (e.g., Fig. 11). For the biogenic isotherm, the samples were equilibrated with CN32 under strictly anaerobic conditions and allowed to incubate for prescribed periods. The aqueous and HCl extractable concentrations of Fe(II) and Co(II) were determined after incubation. The HCl-extractable data were used as a measure of the sorbed concentration for Figures 6 and 11.

The central issue is that the chemical nature of the HCl extracted surface phase on FeOOH is unknown below a fractional reduction of 0.15. Biogenic Co(II) is distributed within this phase, and the solubilization behavior of Co(II) (kinetics and extent) is determined by its surface properties. The biogenic surface phase may be homogeneous or heterogeneous, and contain Fe(II) in various chemical environments ranging from surface complexes, to clusters, to possibly reduced regions deeper within the crystal structure. Measurements of maximum biogenic Fe(II) adsorption density (by HCl extraction) under conditions where biomineralization was not observed indicated a surface concentration that was 1.2 to 1.5 times the Langmuir sorption maxima determined by abiotic spiking (Zachara et al., 2000). Perhaps the biogenic Fe(II) surface phase exhibits significant two- or three-dimensional character promoted by localized bacterial action at the submicron scale that is physicochemically different from that which results from abiotic spiking. Another possibility is that a hydrous magnetite-like surface phase formed that exhibited structural sites conducive to biogenic Co(II) incorporation and that were more effective than hydroxyl sites for retaining Co(II) in the interfacial region.

Because rather high cell concentrations were used in the bioreduction experiments, biosorption of Fe(II) and Co(II) may have occurred giving rise to the appearance of an increase in the sorption selectivity of the residual goethite. We have investigated the sorption of Fe(II) on CN32 (Liu et al., 2000a) and found it to be significant, but not especially strong. The sorption of Fe(II) on CN32 is much less than that on goethite (Liu et al., 2000b). Under the assumption that Co(II) sorbs like Fe(II) to CN32, we used sorption isotherms to calculate (using MINTEQA2) the phase distribution of Co(II) in the mixed system of goethite and CN32, assuming sorption site independence and an additive response. The results (not shown) indicated that biosorption could enhance the Co(II) isotherm by ~0.25 log units; which was below that observed in Figure 11a. While we concluded that biosorption alone, could not account for the enhanced sorptivity of the biogenic Co(II), we note that sorbent mixtures may not behave in additive fashion. Sorbent-sorbent interactions may lead to enhanced sorption affinity over that predicted by an additive model (e.g., Tipping et al., 1983; Davis, 1984; Laxen, 1985).

The data presented in Figure 4b indicated that three out of the four trace metal amended media displayed enhanced Co(II) solubilization (e.g., log $[Co(II)_{(aq)}/Fe(II)_{(aq)}] > -2.0$). Competitive mass action is one explanation for this observation. A mass action effect implies that biogenic Co(II) is in chemical communication (e.g., exchange) with the aqueous phase, and not sequestered deeply in a surface coating. Competitive displacement of biogenic Co(II) is consistent with the abiotic competitive sorption results presented for Co^{2+} in the presence of equimolar Fe^{2+}, where only a small competitive effect was observed at the highest concentrations (Fig. 11b). The lack of competition at equimolar concentration may be rationalized by postulating "partially independent" (stereo-selective) site populations operative over certain concentration ranges (e.g., Benjamin and Leckie, 1981). Higher levels of Fe^{2+} (e.g., 200 : 1) gain access to sites that are intrinsically more selective for Co(II), paving way to a competitive response from trace metals that were present in the media at cumulatively higher concentration.

Precipitation/coprecipitation. The partitioning data for Co(II) plotted in Figure 6 and Figure 11 indicated that Co(II) association with the residual oxide increased with: 1) fractional reduction of FeOOH, and 2) the formation of ferrous iron mineral phases including siderite and vivianite. Coprecipitation of Co(II) within biogenic ferrous iron phases was implied from the concurrent reductions in $Fe^{2+}_{(aq)}$ and $Co^{2+}_{(aq)}$ that occurred at the latter time periods of incubation (Figs. 2 and 3). Coprecipitation can reduce the solubility of an aqueous phase component below that controlled by adsorption or discrete phase solubility reactions.

Siderite ($FeCO_3$) is a rhombohedral carbonate. To a first approximation, the ability of a foreign divalent cation ion to substitute within or to form a solid solution with $FeCO_3$ is dependent upon the similarity of its ionic radius $[r(M^{2+})]$ in octahedral coordination with that of Fe^{2+} $\{[r(M^{2+})] = 0.78$ A°$\}$. Significant miscibility generally requires that $[\Delta r(M^{2+})] \leq 0.11$ (Reeder, 1990). The octahedral ionic radius of both Co(II) (0.72 A°) and Ni(II) (0.69 A°) are such that significant substitution of them in $FeCO_3$ is conceivable. Manganese(II) (0.80 A°) (Rosenberg, 1963) and Zn(II) (0.74 A°) (Bak and Zabinski, 1981) form extensive, continuous solid solutions with $FeCO_3$. Trace-metal analysis of marine siderite cements (Pye, 1984) and sulfide weathering products (Thornber and Nickel, 1976) indicate the presence of both Co(II) and Ni(II). Thornber and Nickel (1976) investigated the coprecipitation of Co^{2+}, Ni^{2+}, and other divalent metals in $FeCO_{3(s)}$ at 23°C and pH 7. Average distribution coefficients (D) of 0.83 and 0.12 were observed for Co^{2+} and Ni^{2+}, respectively. These D values are high enough to allow significant incorporation of Ni^{2+} and Co^{2+} into $FeCO_{3(s)}$ (Rimstidt et al., 1998).

We believe, but were unable to document by analysis, that Co(II) and Ni(II) were incorporated into the siderite formed through bioreduction of the Co-FeOOH and the Ni-FeOOH. We note that Mn(II) [$D = 6.5$; Thornber and Nickel (1976)] and Ca [$D = 0.085$; Thornber and Nickel, (1976)] were incorporated in biogenic $FeCO_3$ produced under laboratory culture conditions similar to those used here (Mortimer et al., 1997). Mortimer et al., (1997), however, showed that the extent of Mn(II) coprecipitation in biogenic siderite was not easily predicted from solution composition and exhibited complex dependency on bacterial respiration and precipitation rates.

The coprecipitation experiment described in Section 3.5 demonstrated that Co(II) can be retained in vivianite. The experimentally measured separation factor ($D = 8.73$) was high enough to justify the increase in Co(II)-K_d that was observed in phosphate containing media with increasing fractional solid phase reduction (Fig. 6). Partial substitution of Co(II) for Fe(II) in vivianite was expected because of the similarity in the ionic radius of Fe(II) and Co(II) as mentioned above, and the ability of both metals, as well as Ni(II), to form isostructural double phosphates [e.g., $Fe_3(PO_4)_2 \cdot 8H_2O$; $Co_3(PO_4)_2 \cdot 8H_2O$, Rudii and Antraptseva, 1991; Trapeznikova et al., 1983; $Ni_3(PO_4)_2 \cdot 8H_2O$, Jambor and Dutrizac, 1995]. The solid solution behavior of vivianite with transition metal cations has apparently not been studied. Double hydrated phosphates of Co(II), Mn(II), and Zn(II), however, undergo extensive solid solution formation with the similarly sized Mg(II) ion $[r(M^{2+}) = 0.72$ A°] (Rudii and Antraptseva, 1991). Similarly, double hydrated arsenates of Co(II) and Ni(II) [e.g., annabergite, $Ni_3(AsO_4)_2 \cdot 8H_2O$; erythite, $Co_3(AsO_4)_2 \cdot 8H_2O$], which are isostructural with the double phosphates, also undergo significant solid solution with themselves and Mg(II) (Jambor and Dutrizac, 1995). This inferential evidence suggests that vivianite may function as a significant repository for Fe(III)-oxide entrained Co(II) and/or Ni(II) that is solubilized by bioreduction. However, as noted above for siderite, the extent of Co(II) and Ni(II) coprecipitation in the biogenic vivianite is unknown and is likely to be controlled by interactive factors related to precipitation mechanism, rate, and location; aqueous concentrations of Co(II) and Ni(II); and microbial effects.

4.4. Role of AQDS

AQDS functions as an electron shuttle for DIRB under certain conditions, accepting electrons generated by respiration and shuttling them to, and enhancing electron transfer at the Fe(III) oxide surface. The mechanism of heterogeneous electron transfer of dihydroanthraquinone disulfonate (AH_2DS) at the oxide-water interface parallels that of hydroquinone, which has been more extensively studied (Stone and Morgan, 1984; LaKind and Stone, 1989; Stone and Ulrich, 1989). In previous studies, the shuttle effect of AQDS has accelerated the rate and extent of both non- and crystalline Fe(III) oxide reduction and influenced the nature of biomineralization products formed (Fredrickson et al., 1998; Zachara et al., 1998). It is not known whether the presence of AQDS eliminates the need for cell-oxide contact, which is required for bacterial Fe(III) oxide reduction in its absence.

Contrary to expectation, AQDS did not significantly enhance the bacterial reduction of the Co- and Ni-FeOOH in the 25-day incubation (Table 5). Perhaps there was slight stimulation in the HCO_3^- buffer experiments where the fractional reduction of both Co-FeOOH and Ni-FeOOH was from 2.7 to 3.8% higher in presence of AQDS (Table 5). The 32-day incubations of Co-FeOOH, whose results were summarized in Figures 2 to 10, were all performed in presence of 100-μM AQDS. The final extent of bioreduction observed in the 32-day incubations of Co-FeOOH ranged from ~25 to 35% of the crystalline oxide depending on buffer and media treatment (Fig. 4a). This reduc-

tion extent exceeded that observed for nonmetal substituted FeOOH of similar surface area in the absence of AQDS (9.2%), but was nearly identical to the reduction extent observed in presence of AQDS (32.8%; Zachara et al., 1998). These latter experiments employed a 39-day incubation period.

An explanation for the lack of stimulation of Co- and Ni-FeOOH reduction by AQDS over the shorter 25-day incubation period was not apparent. Strongly sorbing metal cations, particularly those forming bi- or multinuclear surface complexes, can inhibit the acid dissolution of oxides by reducing surface protonation and blocking active dissolution sites such as those located at kinks or step edges (Hering and Stumm, 1990; Stumm, 1992; Biber et al., 1994). Perhaps structural Co and Ni may function in similar capacity for reductive dissolution by temporally blocking surface sites and slowing initial bioreduction rates. The data from the 32-day incubations with Co-FeOOH, however, indicated that these effects, if indeed present, were short term because the final extents of reduction for Co-FeOOH were comparable to that observed for metal-free goethite in the presence of AQDS.

5. CONCLUSIONS

Metal cations that are co-precipitated or structurally incorporated in FeOOH may be released during bacterial reduction of the crystalline oxide. The presence of Co or Ni in the Fe(III) oxide at the concentration studied (1 mol.%) had no observable influence on the susceptibility of goethite to bioreduction. The trace-metal cations were released from the structure at a concentration and rate, relative to Fe(II), that was proportional to their mole fraction. Redox sensitive [Co(III/II)] and insensitive metals [Ni(II)] behaved in similar fashion, in part because thermodynamics favored bacterial reduction of Co(III) to Co(II). Biogenic Fe(II) strongly associated with the solid phase as an undifferentiated sorption complex on the residual oxide and CN32, and as discrete secondary mineral precipitates. A combination of geochemical reactions including adsorption to the residual Fe(III) oxide and coprecipitation within ferrous iron biomineralization products controlled whether the released metals remained associated with the solids or were solubilized into the aqueous phase. Siderite and vivianite formed when the goethite was appreciably reduced (>15%), and both appeared to structurally incorporate Co(II).

The use of multiple isotopes of Co (^{60}Co, ^{57}Co) allowed us to trace the solid–liquid distribution of both nutrient and oxide entrained Co, and lead us to conclude that Co(II) that was released from the structure was held at the surface more strongly than a Co^{2+} adsorption complex on the goethite surface. The nature of this chemical association or phase was not determined. The highest degree of solubilization occurred in media containing nutrient trace metals, suggesting that sorbed structural ions were in exchange equilibrium with the aqueous phase.

The metal-substituted FeOOH was incompletely reduced in our experiments (≈5–30%), as was noted in previously reported batch studies with iron-reducing bacteria and synthetic goethite (Roden and Zachara, 1996; Urrutia et al., 1998). Complex, unresolved physiologic and surface chemical phenomena appear to control the reduction extent of crystalline Fe(III) oxides. Because structural contaminants are released from FeOOH in proportion to their mole fraction [e.g., Co(III), Ni(II) and like ions], factors that enhance FeOOH bioreduction, such as the presence of Fe(II) complexants (Urrutia et al., 1998) and advective removal of biogenic Fe(II) (Roden and Urrutia, 1999), will accelerate trace metal release and their biogeochemical cycling. We have observed that natural, crystalline Fe(III) oxides are more reducible (Zachara et al., 1998) and adsorb cationic metals more weakly (Zachara et al., 1996; Zachara et al., 1999) than their synthetic counterparts. Structural imperfection and the presence of both structural and surface impurities in the natural Fe(III) oxides are among the many potential reasons for these differences. We may therefore conclude that oxide-entrained trace metals in soil and subsurface environments may be more readily released by dissimilatory iron reduction than observed in this model system study. Whether the biomobilized trace metals remain associated with the solid phase or are solubilized to the aqueous phase and are available for transport will be a complex function of the aqueous and solid-phase geochemical composition controlling the magnitude, nature, and reversibility of adsorption and precipitation reactions.

Acknowledgments—This research was supported by the Natural and Accelerated Bioremediation Research Program (NABIR), Office of Biological and Environmental Research (OBER), of U.S. Department of Energy.

Associate editor: L. M. Walter

REFERENCES

Ainsworth C. C., Girvin D. C., Zachara J. M., and Smith S. C. (1989) Chromate adsorption on goethite: Effects of aluminum substitution. *Soil Sci. Soc. Am. J.* **53,** 411–418.

Al-Borno A. and Tomson M. B. (1994) The temperature dependence of the solubility product constant of vivianite. *Geochim. Cosmochim. Acta* **58,** 5373–5378.

Allison J. D., Brown D. S., and Novo–Gradac K. J. (1991) MINTEQA2/PRODEFA2, A Geochemical Assessment Model for Environmental Systems: Version 3.0 User's Manual. U.S. Environmental Protection Agency.

Bak B. and Zabinski W. (1981) On the continuity of the solid solution series smithsonite-siderite. *Mineralogia Polonica* **13,** 75–80.

Benjamin M. M. and Leckie J. O. (1981) Multiple-site adsorption of Cd, Cu, Zn, and Pb on amorphous iron oxyhydroxide. *J. Colloid Interface Sci.* **79,** 209–221.

Biber M. V., Dos Santos Afonso M., and Stumm W. (1994) The coordination chemistry of weathering: IV. Inhibition of the dissolution of oxide minerals. *Geochim. Cosmochim. Acta* **58,** 1999–2010.

Bousserrhine N., Gasser U. G., Jeanroy E., and Berthelin J. (1999) Bacterial and chemical reductive dissolution of Mn-, Co-, Cr-, and Al-substituted goethites. *Geomicrobiology J.* **16,** 245–258.

Bruno J., Wersin P., and Stumm W. (1992) On the influence of carbonate in mineral dissolution: II. The solubility of $FeCO_{3(s)}$ at 25°C and 1 atm total pressure. *Geochim. Cosmochim. Acta* **56,** 1149–1155.

Clark W. M. (1960) *Oxidation-Reduction Potentials of Organic Systems*. Williams & Wilkins.

Cornell R. M. and Giovanoli R. (1989) Effect of cobalt on the formation of crystalline iron oxides from ferrihydrite in alkaline media. *Clays Clay Miner.* **37,** 65–70.

Cornell R. M. and Schwertmann U. (1996) *The Fe Oxides: Structure, Properties, Reactions, Occurrences, and Uses.* VCH.

Cornell R. M., Giovanoli R., and Schneider W. (1992) The effect of nickel on the conversion of amorphous iron(III) hydroxide into more crystalline iron oxides in alkaline media. *J. Chem. Tech. Biotechnol.* **53,** 73–79.

Davis J. A. (1984) Complexation of trace metals by adsorbed natural organic material. *Geochim. Cosmochim. Acta* **48,** 679–691.

Farley K. J., Dzombak D. A., and Morel F. M. M. (1985) A surface precipitation model for the sorption of cations on metal oxides. *J. Colloid Interface Sci.* **106,** 226–242.

Fredrickson J. K., McKinley J. P., Bjornstad B. N., Ringelberg D. B., White D. C., Krumholz L. R., Suflita J. M., Colwell F. S., Lehman R. M., and Phelps T. J. (1997) Pore-size constraints on the activity and survival of subsurface bacteria in a late Cretaceous shale-sandstone sequence, northwestern New Mexico. *Geomicrobiology J.* **14,** 183–202.

Fredrickson J. K., Zachara J. M., Kennedy D. W., Dong H., Onstott T. C., Hinman N. W., and Li S.-M. (1998) Biogenic iron mineralization accompanying the dissimilatory reduction of hydrous ferric oxide by a groundwater bacterium. *Geochim. Cosmochim. Acta* **62,** 3239–3257.

Fredrickson J. K., Zachara J. M., Kennedy D. W., Duff M. C., Gorby, Y. A., Li S. M., and Krupka K. M. (1999) Reduction of U(VI) in goethite (α-FeOOH) suspensions by a dissimilatory metal-reducing bacterium. *Geochim. Cosmochim. Acta* **64,** 3085–3098.

Gerth J. (1990) Unit-cell dimensions of pure and trace metal-associated goethites. *Geochim. Cosmochim. Acta* **54,** 363–371.

Giovanoli R. and Cornell R. M. (1992) Crystallization of metal substituted ferrihydrites. *Z. Pflanzenernahr. Bodenk.* **155,** 455–460.

Girvin D. C., Gassman P. L., and Bolton H. J. (1996) Adsorption of nitrilotriacetate (NTA), Co, and CoNTA by gibbsite. *Clays Clay Miner.* **44,** 757–768.

Gorby Y. A., Caccavo J. F., and Bolton H., Jr. (1998) Microbial reduction of cobalt^{III}EDTA$^-$ in the presence and absence of manganese(IV) oxide. *Environ. Sci. Technol.* **32,** 244–250.

Greenberg J. and Tomson M. (1992) Precipitation and dissolution kinetics and equilibria of aqueous ferrous carbonate vs temperature. *Appl. Geochem.* **7,** 185–190.

Haderlein S. B. and Pecher K. (1999) Pollutant reduction in heterogeneous Fe(II)-Fe(III) systems. In *Mineral-Water Interfacial Reactions, Vol. 17* (eds. D. L. Sparks and T. J. Grundl), pp. 342–356. American Chemical Society.

Hem J. D., Roberson C. E., and Lind C. J. (1985) Thermodynamic stability of CoOOH and its coprecipitation with manganese. *Geochim. Cosmochim. Acta* **49,** 801–810.

Hering J. G. and Stumm W. (1990) Oxidative and reductive dissolution of minerals. In *Mineral-Water Interface Geochemistry, Vol. 23* (eds. M. F. Hochella and A. F. White), pp. 427–465. Mineralogical Society of America.

Heron G., Crouzet C., Bourg A. C. M., and Christensen T. H. (1994) Speciation of Fe(II) and Fe(III) in contaminated aquifer sediments using chemical extraction techniques. *Environ. Sci. Technol.* **28,** 1698–1705.

Jambor J. L. and Dutrizac J. E. (1995) Solid solutions on the Co-Ni and Ni-Mg joins of the arsenate members of the vivianite group, and their environmental significance. In *Process Mineralogy XIII* (ed. R. D. Hagni), pp. 239–249. The Minerals, Metals and Materials Society.

LaKind J. S. and Stone A. T. (1989) Reductive dissolution of goethite by phenolic reductants. *Geochim. Cosmochim. Acta* **53,** 961–971.

Laxen P. H. (1985) Trace metal adsorption/co-precipitation on hydrous ferric oxide under realistic conditions. *Water Res.* **19,** 1229–1236.

Lim–Nunez R. and Gilkes R. J. (1987) Acid dissolution of synthetic metal-containing goethites and hematites. In *Proceedings International Clay Conference, Denver, 1985*. (eds. L. G. Schultz, H. V. Olphen, and F. A. Mumpton), pp. 197–204. Clay Mineralogical Society.

Lindsay W. L. (1979) *Chemical Equilibria in Soils*. Wiley-Interscience.

Liu C., Zachara J. M., Szecsody J. E., Gorby Y. A., and Brown C. (2000a) Coupled microbial reduction of Fe^{3+} and sorption of Fe^{2+} on bacterium, *S. putrefaciens*, CN32. *Environmental Science and Technology* (in press).

Liu C., Kota S., Zachara J. M., Fredrickson J. K., Brinkman C. K. (2000b) Kinetic analysis of the bacterial reduction of goethite. *Environmental Science and Technology* (in press).

Lovley D. R. (1993) Dissimilatory metal reduction. *Ann. Rev. Microbiol.* **47,** 263–290.

Lovley D. R. and Phillips E. J. P. (1986) Organic matter mineralization with reduction of ferric iron in anaerobic sediments. *Appl. Environ. Micro.* **51,** 683–689.

Lovley D. R., Phillips E. J. P., and Lonergan D. J. (1991) Enzymatic versus nonenzymatic mechanisms for Fe(III) reduction in aquatic sediments. *Environ. Sci. Technol.* **25,** 1062–1067.

Lovley D. R., Coates J. D., Blunt–Harris E. L., Phillips E. J. P., and Woodward J. C. (1996) Humic substances as electron acceptors for microbial respiration. *Nature* **382,** 445–448.

Lovley D. R., Fraga J. L., Blunt–Harris E. L., Hayes L. A., Phillips E. J. P., and Coates J. D. (1998) Humic substances as a mediator for microbially catalyzed metal reduction. *Acta Hydrochim. Hydrobiol.* **26,** 152–157.

McArdell C. S., Stone A. T., and Tian J. (1998) Reaction of EDTA and related aminocarboxylate chelating agents with Co(III)OOH (Heterogenite) and Mn(III)OOH (Manganite). *Environ. Sci. Technol.* **32,** 2923–2930.

Mortimer R. J. G. and Coleman M. L. (1997) Microbial influence on the isotopic composition of diagenetic siderite. *Geochim. Cosmochim. Acta* **61,** 1705–1711.

Mortimer R. J. G., Coleman M. L., and Rae J. E. (1997) Effect of bacteria on the elemental composition of early diagenetic siderite: implications for palaeoenvironmental interpretations. *Sedimentology* **44,** 759–765.

Naumov G. B., Ryzhenko B. N., and Kodakovsky I. L. (1974) Handbook of Thermodynamic Data. N.T.I.S. Report No. USGS-WRD-74-001.

Olsen S. R. and Sommers L. E. (1982) Phosphorous. In *Methods of Soil Analysis, Part 2—Chemical and Microbiological Properties* (eds. L. Page, R. H. Miller, and D. R. Keeney), pp. 403–430. American Society for Agronomy.

Postma D. (1981) Formation of siderite and vivianite and the pore-water composition of a recent bog sediment in Denmark. *Chem. Geol.* **31,** 225–244.

Pye K. (1984) SEM analysis of siderite cements in intertidal marsh sediments, Norfolk, England. *Marine Geol.* **56,** 1–12.

Pye K., Dickson J. A. D., N. S., Coleman M. L., and Cox M. (1990) Formation of siderite-Mg-calcite-iron sulphide concretions in intertidal marsh and sandflat sediments, north Norfolk, England. *Sedimentology* **37,** 325–343.

Reeder R. J. (1990) Crystal chemistry of the rhombohedral carbonates. In *Carbonates: Mineralogy and Chemistry, Vol. 11* (ed. R. J. Reeder), pp. 1–48. Mineralogical Society of America.

Rimstidt J. D., Balog A., and Webb J. (1998) Distribution of trace elements between carbonate minerals and aqueous solutions. *Geochim. Cosmochim. Acta* **62,** 1851–1863.

Roden E. E. and Urrutia M. M. (1999) Ferrous iron removal promotes microbial reduction of crystalline iron(III) oxides. *Environ. Sci. Technol.* **33,** 1847–1853.

Roden E. E. and Zachara J. M. (1996) Microbial reduction of crystalline Fe(III) oxides: influence of oxide surface area and potential for cell growth. *Environ. Sci. Technol.* **30,** 1618–1628.

Rosenberg P. E. (1963) Synthetic solid solutions in the systems $MgCO_3$-$FeCO_3$ and $MnCO_3$-$FeCO_3$. *Am. Mineral.* **48,** 1396–1400.

Rudii I. V. and Antraptseva N. M. (1991) Solubility and thermodynamic characterization of double hydrated phosphates of certain divalent metals. *Russian J. Inorg. Chem.* **36,** 1565–1568.

Sawicki J. A., Brown D. A., and Beveridge T. J. (1995) Microbial precipitation of siderite and photoferrihydrite in a biofilm. *Canadian Mineral.* **33,** 1–6.

Schindler P. W. and Stumm W. (1987) The surface chemistry of oxides, hydroxides, and oxide minerals. In *Aquatic Surface Chemistry* (ed. W. Stumm), pp. 83–110. John Wiley & Sons.

Schwertmann U. and Taylor R. M. (1989) Iron oxides. In *Minerals in Soils Environments, 2nd ed. Soil Science Society American Journal Book Series No. 1* (eds. J. B. Dixon and S. B. Weed), pp. 379–438.

Schwertmann U. (1991) Solubility and dissolution of iron oxides. *Plant Soil* **130,** 1–25.

Scott D. T., McKnight D. M., Blunt–Harris E. L., Kolesar S. E., and Lovely D. R. (1998) Quinone moieties act as electron acceptors in the reduction of humic substances by humics-reducing microorganisms. *Environ. Sci. Technol.* **32,** 2984–2989.

Singh B. and Gilkes R. J. (1992) Properties and distribution of iron

oxides and their association with minor elements in the soils of south-western Australia. *J. Soil Sci.* **43,** 77–98.
Smith R. A. and Martell A. E. (1997) NIST Critically Selected Stability Constants of Metal Complexes Database. *Version 3.0*. User's Guide and Database Software. NIST Standard Reference Database No. 46. U.S. Department of Commerce.
Sposito G. (1981) *The Thermodynamics of Soil Solutions*. Oxford University Press.
Stone A. T. and Morgan J. J. (1984) Reduction and dissolution of manganese(III) and manganese(IV) oxides by organics. 1. Reaction with quinone. *Environ. Sci. Technol.* **18,** 450–456.
Stone A. T. and Ulrich H. J. (1989). Kinetics and reaction stoichiometry in the reductive dissolution of manganese(IV) dioxide and Co(III) oxide by hydroquinone. *J. Colloid Interface Sci.* **132,** 509–515.
Stookey L. L. (1970) Ferrozine-A new spectrophotometric reagent for iron. *Anal. Chem.* **42,** 779–781.
Stumm W. (1992) *Chemistry of the Solid-Water Interface*. John Wiley & Sons.
Stumm W. and Sulzberger B. (1992) The cycling of iron in natural environments: considerations based on laboratory studies of heterogeneous redox processes. *Geochim. Cosmochim. Acta* **56,** 3233–3257.
Thornber M. R. and Nickel E. H. (1976) Supergene alteration of sulphides. III. The composition of associated carbonates. *Chem. Geol.* **17,** 45–72.
Tipping E., Griffith J. R., and Hilton J. (1983) The effect of adsorbed humic substances on the uptake of copper(II) by goethite. *J. Groat. Chim. Acta* **56,** 613–621.
Torrent J., Schwertmann U., and Barron V. (1987) The reductive dissolution of synthetic goethite and hematite in dithionite. *Clays Clay Miner.* **22,** 329–337.
Trapeznikova L. V., Shestidesyatnaya N. L., and Karnaukhov A. I. (1983) Solubility of crystalline hydrated zinc, cobalt, and copper normal orthophosphates. *Russian J. Inorg. Chem.* **28,** 2394–2397.
Trolard F. and Tardy Y. (1987) The stabilities of gibbsite, boehmite, aluminous goethites and aluminous hematites in bauxites, ferricretes and laterites as a function of water activity, temperature and particle size. *Geochim. Cosmochim. Acta* **51,** 945–957.
Trolard F., Bourrie G., Jeanroy E., Herbillon A. J., and Martin H. (1995) Trace metals in natural iron oxides from laterites: A study using selective kinetic extraction. *Geochim. Cosmochim. Acta* **59,** 1285–1297.
Urrutia M. M., Roden E. E., Fredrickson J. K., and Zachara J. M. (1998) Microbial and surface chemistry controls on reduction of synthetic Fe(III)-oxide minerals by the dissimilatory iron-reducing bacterium *Shewanella alga*. *Geomicrobiology* **15,** 269–291.
Zachara J. M., Fredrickson J. K., Urrutia M. M., and Gorby Y. (1996) Surface chemical metering of bacterial iron oxide reduction and effects of reduction on Fe(III)-oxide reactive surface chemistry. *The 1996 International Symposium on Subsurface Microbiology*, p. 102.
Zachara J. M., Fredrickson J. K., Li S.-M., Smith S. C., and Gassman P. L. (1998) Bacterial reduction of crystalline Fe(III) oxides in single phase suspensions and subsurface materials. *Am. Mineral.* **83,** 1426–1443.
Zachara J. M., Smith S. C., and Fredrickson J. M. (2000) The effect of biogenic Fe(II) on the stability and sorption of Co(II)EDTA^{2-} to goethite and a subsurface sediment. *Geochim. Cosmochim. Acta* **64,** 1345–1362.

Table A1. Results of ICP-AES analysis (μg/mL) of the aqueous phase after 32-day incubation of Co-FeOOH with CN32.

Element	Media #1	Media #2	Media #3	Media #4	Media #5	Media #6
Al	<0.03	<0.03	<0.03	<0.03	<0.03	<0.03
Ca	6.61	3.56	22.4	27.2	16.4	2.86
Co	1.13	1.26	0.80	1.09	0.43	0.47
Cu	<0.006	<0.006	<0.006	<0.006	<0.006	<0.006
Fe	18.1	32.3	21.4	108	30.2	25.1
K	56.2	49.2	56.2	53.4	55.6	51.6
Mg	1.63	3.02	0.98	3.16	<0.06	<0.06
Mn	<0.02	<0.02	0.03	1.46	<0.02	<0.02
Na	2407	2269	2166	2031	2417	2261
Ni	<0.02	<0.02	<0.02	<0.02	<0.02	<0.02
P	1.67	0.48	0.52	0.01	0.58	<0.08
S	12.7	12.4	110	100	.06	7.50
Si	12.0	9.48	7.92	5.83	11.4	9.25
Zn	<0.05	<0.05	<0.05	<0.05	<0.05	<0.05